Geophys. J. R. astr. Soc. (1987) 89, 579–636

Some remarks on the Gaussian beam summation method

B. S. White,* A. Norris,‡ A. Bayliss* and R. Burridge†

* *Exxon Research and Engineering Company, Corporate Research Science Laboratories, Clinton Township, Route 22 East, Annandale, New Jersey 08801, USA*
† *Courant Institute of Mathematical Sciences, New York University, NY 10012, USA*
‡ *Rutgers University, Department of Mechanics and Materials Science, PO Box 909, Piscataway, NJ 08854, USA*

Accepted 1986 September 25. Received 1986 September 25; in original form 1985 December 23

Summary. Recently, a method using superposition of Gaussian beams has been proposed for the solution of high-frequency wave problems. The method is a potentially useful approach when the more usual techniques of ray theory fail: it gives answers which are finite at caustics, computes a non-zero field in shadow zones, and exhibits critical angle phenomena, including head waves. Subsequent tests by several authors have been encouraging, although some reported solutions show an unexplained dependence on the 'free' complex parameter ϵ which specifies the initial widths and phases of the Gaussian beams.

We use methods of uniform asymptotic expansions to explain the behaviour of the Gaussian beam method. We show how it computes correctly the entire caustic boundary layer of a caustic of arbitrary complexity, and computes correctly in a region of critical reflection. However, the beam solution for head waves and in edge-diffracted shadow zones are shown to have the correct asymptotic form, but with governing parameters that are explicitly ϵ-dependent. We also explain the mechanism by which the beam solution degrades when there are strong lateral inhomogeneities. We compare numerically our predictions for some representative model problems, with exact solutions obtained by other means.

Key words: ray theory, caustics, diffraction, head waves

1 Introduction

The Gaussian beam summation method for fast asymptotic solution of high frequency wave problems has attracted much attention, especially in the geophysical community, since its recent proposal by Červený, Popov & Pšenčík (1982) and Popov (1982). In this paper we use

25

techniques from the theory of uniform asymptotic expansions to explain the sometimes anomalous behaviour of this potentially powerful method. For several canonical problems, in 2-D with piece-wise homogeneous media, we compare numerical computations obtained by Gaussian beam summation with trusted solutions obtained by other means.

The Gaussian beam method bears many similarities to that of asymptotic ray theory: the centre lines, or axes, of the Gaussian beams follow ray-paths, and the auxiliary ordinary differential equations which must be solved along the ray-paths for implementation of the beam method are identical, except for initial conditions, to those that are routinely integrated in dynamic ray-tracing programmes. These initial conditions are real for a ray but complex-valued for a beam. In fact, a single Gaussian beam may be understood as a bundle of rays travelling in complex space near the beam axis, which propagates in real space (Keller & Streifer 1971; Deschamps 1971). To synthesize asymptotically the field of a point source, one must first trace beams emanating from the source at all take-off angles, θ. The field of the point source is then obtained by integration (summation) over θ.

The beam method promises several advantages over rays. Most notably, it has been used to compute in singular regions, e.g. caustics, shadow zones, and regions of critical and post-critical reflection, where naive ray theory is invalid. Although modifications to ray theory are available to correct these difficulties, their implementation can be somewhat involved. In contrast, the beam method has been proposed to handle singular regions, and even arbitrary overlaps of singular regions, without modification (Červený *et al.* 1982).

While numerical computations by several authors have tended to confirm the general applicability of the method, discrepancies have also been reported. Caustic calculations compare favourably with the Airy function modification of ray theory (Červený *et al.* 1982; Nowack & Aki 1985). Critical angle and head wave calculations by Gaussian beams have matched excellently with exact solutions obtained by separation of variables (Konopaskova & Červený 1984, I & II). Edge diffraction has been computed numerically by Gaussian beams (Nowack & Aki 1985; Červený 1983) and the results described as 'promising' (Červený 1983). In addition several authors (e.g. Nowack & Aki 1985; Cormier & Spudich 1984) computed wavefields for rather complex geological structures, and reported reasonable results using the method.

However, consistency checks on the Gaussian beam solution using source–receiver reciprocity (Müller 1984) were not completely successful, leading that author to conclude that the beam method is not valid when there are strong lateral inhomogeneities. Also, some reported solutions show a marked dependence on the 'free' complex parameter ϵ which characterizes the initial widths and phases of the Gaussian beams. This parameter, an artefact of the beam superposition method, does not enter into the formulation of the wave problem being solved, and the theory predicts that its choice will not affect the Gaussian beam result in the high-frequency limit. None the less some phenomena, e.g. edge diffraction and head waves, cannot be obtained at all for some values of ϵ (Nowack & Aki 1985; Červený 1983). The role of ϵ has been investigated by several authors, e.g. Madariaga (1984).

A systematic study of the range of validity of the Gaussian beam method was undertaken by Ben-Menahem & Beydoun (1985) and Beydoun & Ben-Menahem (1985), who concluded with seven inequalities. However, these authors did not take into account the various canonical integrals arising from the uniform asymptotic expansion of the beam superposition integral. Thus, we are able to exhibit cases for which their conditions are not sufficient. In particular, their Fresnel-2 condition may sometimes be interpreted as the physically reasonable requirement that the beam width at an interface be much smaller than the radius of curvature of the interface. However, neither this nor the full Fresnel condition explains our results for reflections from a circular cylinder.

Ray theory in a non-singular region can be formally obtained from beam superposition by a saddle point evaluation of the beam superposition integral. In Section 5 we show how the beam integral correctly captures the entire caustic boundary layer of a caustic of arbitrary complexity, through a coalescence of nearby saddle points. As an example, we compute reflections from a syncline, and compare the results with those of ray theory, and with accurate calculations based on the Kirchhoff integral and on a careful finite difference computation. On the dark side of the caustic, where the boundary layer persists for several wavelengths, the beams correctly compute a change in pulse shape not accounted for by naive ray theory. We show how an extra oscillation in the pulse is caused by a pair of saddle points in the complex plane which are not accessible to ray theory. We relate these phenomena to the more familiar Kirchhoff integral, whose asymptotics are shown to be identical to those of the integral studied here.

In Section 6 we investigate the deterioration of the beam solution when there are strong lateral variations. For reflections from a circular cylinder, a problem with an exact solution obtainable by separation of variables, the lateral variations can be controlled by changing the cylinder diameter. We show how inaccuracies are introduced into the beam integral by a pair of spurious saddles in the complex plane. In contrast with the complex saddles mentioned above in relation to the caustic, these spurious saddles are a non-physical artefact of the beam method, and are a source of ϵ-dependence in the uniform asymptotic expansion. We demonstrate how a judicious choice of ϵ can neutralize the effects of the spurious saddles and restore accuracy to the beam solution. In Section 7, we use insight gained from the cylinder problem to improve the accuracy of the beam solution for the syncline problem of Section 5, by a new choice of ϵ.

Critical angle phenomena and head waves are discussed in Section 8. We show how the uniform expansion of the beam integral is governed by the canonical integral for the coalescence of a saddle point with a branch point. An exact solution, obtained by separation of variables, is asymptotically of the same canonical form. However, the controlling parameters of the exact solution are not the same as those for the beam integral, which are shown to have explicit ϵ-dependence. The beam integral is shown to give accurate results very near the critical angle. However, as the observation point moves farther past critical, the correct result is obtained only in the limit $\epsilon \to \infty$. We thereby offer an explanation of the computer results obtained by other authors (Červený 1983; Konopaskova & Červený 1984, I & II; Nowack & Aki 1985).

We obtain analogous results in Section 9 for edge diffraction by considering the classical problem of diffraction by a screen, a problem for which the exact solution was first obtained by Sommerfield (1896). Here the beams give a solution of the correct functional form, but again the controlling parameter is explicitly ϵ-dependent. The situation is thus reminiscent of earlier attempts to compute edge diffraction by Kirchhoff and related methods; these methods also give the correct form, but incorrect parameters (Keller, Lewis & Seckler 1957). However, for this problem the beam integral is exact if ϵ is chosen to be a specific function of receiver position. Similar difficulties will enter into problems with pinch-outs, and artificial edges introduced by numerical approximations of smooth interfaces. Included in this class of problems are the spurious end effects noted by, e.g. Nowack & Aki (1985), which come from a truncation of the range of θ in the beam integral, i.e. by considering a limited range of take-off angles.

In Sections 2–4 we give a self-contained derivation of the 2-D beam and beam superposition formulae, including a new result (equation 4.11), which is used to compute the spurious saddles. In our derivation we avoid the more usual, but unnecessary, intermediary of a parabolic equation approximation, and instead obtain directly the paraxial approximation to the equations of inhomogeneous wave tracking. We thus complete in general the calculations of Choudhary & Felsen (1974), which were for a homogeneous medium. The method originated, in another context, in the paper of Keller (1958).

2 The Gaussian beam

We study solutions of the Helmholtz equation in R^2:

$$\nabla \cdot (\mu \nabla u) + \rho\omega^2 u = 0 \tag{2.1}$$

which, asymptotically, are of WKB form

$$u \sim V \exp(i\omega\phi) \tag{2.2}$$

as $\omega \to \infty$. Here ϕ is called the phase, or eikonal, and V is the amplitude. The particular form of (2.1) governs *SH* waves in plane elastic systems where ρ, μ are density and shear modulus. Substituting (2.2) into (2.1), and equating the coefficients of ω^2, ω to zero yields the familiar eikonal and transport equations of ray theory:

$$\nabla\phi \cdot \nabla\phi = \frac{1}{c^2} \tag{2.3}$$

$$2\nabla\phi \cdot \nabla V + \left(\Delta\phi + \frac{1}{\mu}\nabla\phi \cdot \nabla\mu\right) V = 0, \tag{2.4}$$

where $c = (\mu/\rho)^{1/2}$.

To obtain a solution of (2.1) which represents a beam, we will see that it is sufficient to allow ϕ to be complex. Thus if $\phi = \phi_1 + i\phi_2$ with ϕ_1, ϕ_2 real, we have from (2.3)

$$(\nabla\phi_1)^2 - (\nabla\phi_2)^2 = \frac{1}{c^2} \tag{2.5a}$$

$$\nabla\phi_1 \cdot \nabla\phi_2 = 0. \tag{2.5b}$$

Equations (2.5) are the equations of inhomogeneous wave tracking, investigated by Felsen (1976, 1984). For a solution bounded as $\omega \to \infty$ it is necessary that $\phi_2 > 0$ everywhere to prevent exponential growth. Similarly, if u is not exponentially small everywhere the set $\{x : \phi_2 = 0\}$ is not empty, and we assume it is a smooth curve $\bar{x}(s)$, parameterized by arc-length s. Since u is exponentially concentrated near $\bar{x}$, u represents a beam and $\bar{x}$ is the beam axis.

Now from (2.5b), $\nabla\phi_1[\bar{x}(s)]$ is in the direction of $\bar{x}$. Also, since $\nabla\phi_2 = 0$ on $\bar{x}$, (2.5a) implies that $c\nabla\phi_1$ is a unit vector there. Hence, the unit tangent to $\bar{x}$ is

$$\frac{d}{ds}\bar{x}(s) = c[\bar{x}(s)]\, \nabla\phi_1[\bar{x}(s)]. \tag{2.6}$$

Let

$$P(s) = \nabla\phi_1[\bar{x}(s)] = \nabla\phi[\bar{x}(s)]. \tag{2.7}$$

If we differentiate (2.7) with respect to s, and (2.3) with respect to x and combine the

results to eliminate second derivatives of ϕ, we obtain

$$\frac{d}{ds}\bar{x}(s) = c[\bar{x}(s)]\, P(s) \tag{2.8a}$$

$$\frac{d}{ds}P(s) = -\frac{\nabla c[\bar{x}(s)]}{c[\bar{x}(s)]^2}, \tag{2.8b}$$

Equations (2.8) are the ray equations of ordinary ray theory. Hence the beam axis must be a ray-path. We may write the ray equations in terms of the unit tangent vector $U_1 = cP$ and the unit vector U_2 orthogonal to U_1:

$$\frac{d}{ds}\bar{x}(s) = U_1 \tag{2.9a}$$

$$\frac{d}{ds}U_1(s) = -\frac{(\nabla c \cdot U_2)}{c}\, U_2 \tag{2.9b}$$

To equations (2.9) we may append

$$\frac{d}{ds}\phi[\bar{x}(s)] = \frac{1}{c[\bar{x}(s)]}$$

or

$$\phi = \int_0^s \frac{ds'}{c[\bar{x}(s')]} \tag{2.10}$$

obtained by the chain rule and the identification $U_1 = c\nabla\phi$ obtained from (2.6) and (2.9a).

We now calculate second derivatives of ϕ along $\bar{x}$. First differentiation of (2.3) along $\bar{x}$ yields

$$\nabla\nabla\phi \cdot U_1 = -\frac{\nabla c}{c^2} \tag{2.11}$$

Next, by analogy with dynamic ray theory, we define the 'complex wavefront curvature', $K(s)$, at $\bar{x}(s)$ as

$$K = c\, U_2^T\, \nabla\nabla\phi U_2. \tag{2.12}$$

In terms of K we can write the matrix of second derivatives of the eikonal along $\bar{x}$, in the basis U_1, U_2:

$$[\nabla\nabla\phi]_{\{U_1, U_2\}} = \begin{bmatrix} -\dfrac{\nabla c \cdot U_1}{c^2} & -\dfrac{\nabla c \cdot U_2}{c^2} \\ -\dfrac{\nabla c \cdot U_2}{c^2} & \dfrac{K}{c} \end{bmatrix}. \tag{2.13}$$

A propagation equation for K is easily derived by differentiation of (2.12), use of (2.9), (2.13) and then the second derivative of equation (2.3) to eliminate third derivatives of ϕ. The result is

$$\frac{d}{ds}K(s) = -K^2 + \frac{\nabla c \cdot U_1}{c} K - U_2^T \frac{\nabla\nabla c}{c} U_2. \tag{2.14}$$

Let

$$K(s) = B(s)/A(s) \tag{2.15a}$$

$$B(s) = \frac{d}{ds} A(s). \tag{2.15b}$$

Here A is a 'complex ray-tube area', analogous to the real ray-tube area of ordinary ray theory. The substitution (2.15) linearizes the Riccati equation (2.14):

$$\frac{dA}{ds} = B$$

$$\frac{dB}{ds} = -\left(U_2^T \frac{\nabla\nabla c}{c} U_2\right) A + \frac{\nabla c \cdot U_1}{c} B \tag{2.16}$$

To solve the transport equation (2.4) along $\bar{x}$, note that $\Delta\phi$ is the trace of the matrix in (2.13), and $\nabla\phi = U_1/c$. Then (2.4) becomes

$$\nabla V \cdot U_1 + \frac{V}{2}\left(\frac{B}{A} - \frac{\nabla c \cdot U_1}{c} + \frac{\nabla\mu \cdot U_1}{\mu}\right) = 0 \tag{2.17}$$

From (2.17), (2.9) and (2.16) we obtain

$$\frac{d}{ds} \log \frac{\mu V^2 A}{c} = 0 \tag{2.18}$$

Hence $\mu V^2 A/c$ is conserved along $\bar{x}$, and

$$V(s) = \sqrt{\frac{c(s)\,\mu(s_0)\,A(s_0)}{c(s_0)\,\mu(s)\,A(s)}}\; V(s_0), \tag{2.19}$$

where the branch of the square root is such that V varies continuously in s. By linearity of the Helmholtz equation, $V(s_0)$ is arbitrary. For the validity of (2.19) it must be checked that $A(s) \neq 0$. Thus, let $(A_1, B_1)^T$, $(A_2, B_2)^T$ be linearly independent solutions of (2.16) with initial conditions

$$\begin{pmatrix} A_1 \\ B_1 \end{pmatrix}_{s=0} = \begin{pmatrix} 0 \\ 1 \end{pmatrix}, \quad \begin{pmatrix} A_2 \\ B_2 \end{pmatrix}_{s=0} = \begin{pmatrix} 1 \\ 0 \end{pmatrix}. \tag{2.20}$$

Notice that since equations (2.16) are real so are the solutions $(A_1, B_1)^T$, $(A_2, B_2)^T$. Let

$$\epsilon = \epsilon_1 + i\,\epsilon_2, \qquad \epsilon_1, \epsilon_2 \text{ real}, \epsilon_2 < 0 \tag{2.21}$$

and let $(A, B)^T$ be the solution of (2.16) with initial condition

$$\begin{pmatrix} A \\ B \end{pmatrix}_{s=0} = \begin{pmatrix} \epsilon \\ 1 \end{pmatrix}. \tag{2.22}$$

Thus $A = A_1 + \epsilon A_2$, $B = B_1 + \epsilon B_2$.

Clearly $A \neq 0$ since otherwise $A_1 = A_2 = 0$ which contradict the linear independence of

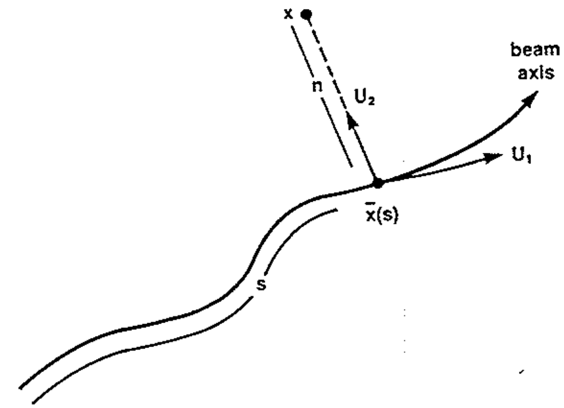

Figure 1. Beam and beam coordinates.

the two solutions in (2.20). Furthermore, from (2.16) we verify the Wronskian relation

$$W(s) = \frac{A_1 B_2 - A_2 B_1}{c(s)} = \frac{-1}{c(s_0)}. \tag{2.23}$$

is conserved along a ray.

We next derive the *paraxial approximation* for u, that is, we use a two-term Taylor series approximation to the eikonal in a neighbourhood of the beam axis. Thus, for a fixed point x near $\bar{x}$, let n be the normal distance from x to $\bar{x}(\cdot)$, i.e. (see Fig. 1).

$$x = \bar{x}(s) + n\,U_2(s). \tag{2.24}$$

Clearly, such a representation of x will be possible only in a sufficiently narrow neighbourhood of the beam axis not intersecting its evolute. Using the derivatives of ϕ, from (2.13), (2.15) we obtain

$$\phi(x) = \phi[\bar{x}(s)] + \frac{1}{2} n^2 \frac{B}{Ac} + 0(n^3). \tag{2.25}$$

Using the Wronskian (2.23), we find that

$$\operatorname{Im} \frac{B}{A} = \operatorname{Im} \frac{(B_1 + \epsilon B_2)}{(A_1 + \epsilon A_2)} = \frac{-\epsilon_2[c(s)/c(s_0)]}{[(A_1 + \epsilon_1 A_2)^2 + \epsilon_2^2 A_2^2]}. \tag{2.26}$$

Thus, from (2.26), (2.25), (2.21) we obtain $\phi_2 > 0$ in this approximation.

To summarize, the paraxial approximation is of the form

$$u \sim V(s_0) \sqrt{\frac{c(s)\,\mu(s_0)\,A(s_0)}{c(s_0)\,\mu(s)\,A(s)}} \exp\left[i\omega\left(\phi[\bar{x}(s)] + \frac{1}{2} n^2 \frac{B}{Ac}\right)\right] \tag{2.27}$$

and is valid for $n = 0(\omega^{-1/2})$, by virtue of the error estimate in (2.25). From (2.27)

$$|u| \sim |V| \exp\left(-\frac{1}{2} \frac{n^2}{L^2}\right) \tag{2.28}$$

with

$$L = \left(\frac{\omega}{c(s)} \operatorname{Im} \frac{B}{A}\right)^{-1/2}. \tag{2.29}$$

Thus in the paraxial approximation there is a Gaussian decay of $|u|$ as n increases away from the beam axis, and a paraxial beam is a Gaussian beam. The beam width L of (2.29) is $O(\omega^{-1/2})$. This defines the region where ϕ is well approximated by its Taylor series truncated after the quadratic terms.

3 Transmission and reflection at interfaces

Let $\bar{Z}(\xi)$ be a smooth interface, parameterized by arclength ξ, across which $c(x)$ is discontinuous. Let $V^{(I)} \exp(i\omega\phi^{(I)})$ be a beam incident on $\bar{Z}(\cdot)$. For simplicity, we assume u is continuous, but allow for a jump in the normal derivative. The interface conditions are satisfied asymptotically as $\omega \to \infty$, by introducing reflected and transmitted beams, $V^{(R)} \exp(i\omega\phi^{(R)})$, $V^{(T)} \exp(i\omega\phi^{(T)})$ on opposite sides of the interface (see Fig. 2), whose beam axes strike the interface at the same point ξ_0 as the axis of the incident beam.

Continuity of u implies that along $\bar{Z}(\cdot)$,

$$V^{(I)} \exp(i\omega\phi^{(I)}) + V^{(R)} \exp(i\omega\phi^{(R)}) = V^{(T)} \exp(i\omega\phi^{(T)}). \tag{3.1}$$

Since (3.1) must be satisfied as $\omega \to \infty$, we conclude that

$$\phi^{(I)}[\bar{Z}(\xi)] = \phi^{(R)}[\bar{Z}(\xi)] = \phi^{(T)}[\bar{Z}(\xi)]. \tag{3.2}$$

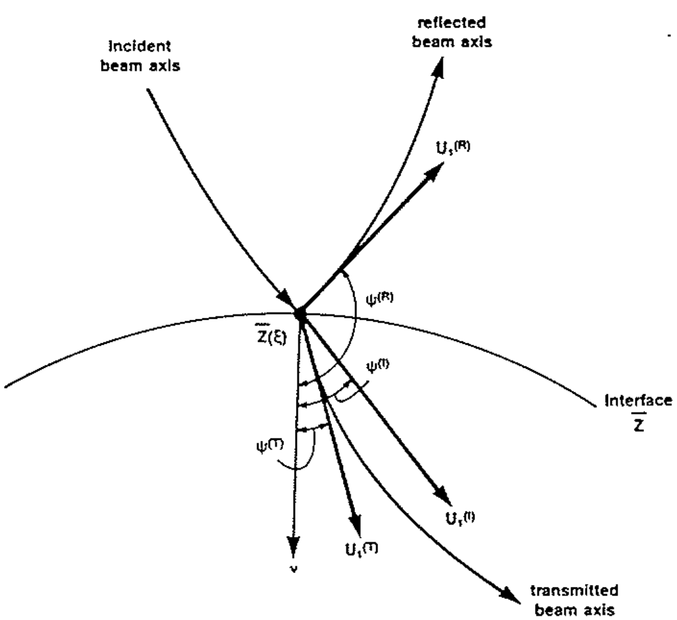

Figure 2. Incident, reflected, and transmitted beams at an interface.

Let ϕ represent one of $\phi^{(I)}, \phi^{(R)}, \phi^{(T)}$. Then (3.2) states that ϕ is conserved on reflection and transmission. Of course, ϕ must also satisfy the equations of Section 2. In particular, $\nabla\phi = U_1/c$ along the beam axis. Differentiation of (3.2) at $\xi = \xi_0$, and identification of $(d/d\xi)\bar{Z}$ with the unit tangent, T, to the interface then yields that the tangential component of slowness U_1/C is conserved, i.e.

$$\frac{T \cdot U_1}{c} \tag{3.3}$$

is conserved.

We say a quantity is conserved at an interface if it is the same for a derived ray as for the incident ray.

Let $\psi^{(I)}, \psi^{(R)}, \psi^{(T)}$ be, respectively, the angles of incidence, reflection, and transmission measured between the ray direction corresponding to the beam axis, and the normal to the interface ν for which $\nu \cdot U_1 > 0$ for the incident field. Then (3.3) expresses the fact that $\sin\psi/c$ is conserved on reflection and transmission. Hence if $c^{(I)}$ is the value of c on the incident side of the interface, $c^{(T)}$ on the transmitted side,

$$\sin\psi^{(I)} = \sin\psi^{(R)}$$

$$\frac{\sin\psi^{(I)}}{c^{(I)}} = \frac{\sin\psi^{(T)}}{c^{(T)}}. \tag{3.4}$$

Equations (3.4) are the familiar law of reflection and Snell's law from ray theory. We may similarly derive other beam formulae identical to those of ray theory. Let a be the radius of curvature of the interface at $\xi = \xi_0$. Then, by taking second derivatives of (3.2) at $\xi = \xi_0$, using (2.13) and the first Frenet formula we find that

$$-\sin^2\psi \frac{\nabla c \cdot U_1}{c^2} - \frac{2\nabla c \cdot U_2}{c^2}(\sin\psi\cos\psi) + \frac{K}{c}\cos^2\psi + \frac{\cos\psi}{ac} \tag{3.5}$$

is conserved.

Expression (3.5) may be used to derive jump conditions for the 'complex wavefront curvatures' $K^{(R)}, K^{(T)}$ of the reflected and transmitted beams, in terms of $K^{(I)}$ for the incident beam. There is, however, an arbitrariness in the jump conditions imposed on A, B, since only their ratio $K = B/A$ is constrained by (3.5). We resolve this ambiguity by requiring $A/\cos\psi$ to be conserved on reflection and transmission. This extra condition is suggested by analogy with ray theory, where it is a geometric fact implied by (3.4). We write the conditions in full only for boundaries between piece-wise homogeneous media, where $\nabla c = 0$. They are

$$A^{(R)} = -A^{(I)}$$

$$B^{(R)} = -B^{(I)} - \frac{2}{a\cos\psi^{(I)}} A^{(I)}$$

$$A^{(T)} = \frac{\cos\psi^{(T)}}{\cos\psi^{(I)}} A^{(I)} \tag{3.6}$$

$$B^{(T)} = \frac{1}{a}\left(\frac{c^{(T)}}{c^{(I)}\cos\psi^{(T)}} - \frac{1}{\cos\psi^{(I)}}\right) A^{(I)} + \frac{c^{(T)}\cos\psi^{(I)}}{c^{(I)}\cos\psi^{(T)}} B^{(I)}. \tag{3.7}$$

(For more general media see Hubral 1980.)

It may now be verified that the Wronskian relation (2.23) remains valid even after reflection and transmission via (3.6) and (3.7). Hence (2.26) is also valid, and the condition $\phi_2 > 0$ (for boundedness) is satisfied, at least in the paraxial approximation (2.27).

With the exception of $V(s_0)$, all functions in (2.27) needed for starting a reflected or transmitted beam in the paraxial approximation have been determined. To get conditions on V, we put (3.2) into (3.1) to yield

$$V^{(I)} + V^{(R)} = V^{(T)}, \tag{3.8}$$

on $\bar{Z}$.

We assume a jump condition on the normal derivative of u of the form

$$\mu_+(\nu \cdot \nabla u)^+ = \mu_-(\nu \cdot \nabla u)^- \tag{3.9}$$

on Z, where μ_+, μ_- are given constants (or functions) and ν is the normal to the interface. Differentiation of (3.1) then yields, to leading order in ω

$$\mu_-\left(V^{(I)}\frac{\cos\psi^{(I)}}{c^{(I)}} - V^{(R)}\frac{\cos\psi^{(R)}}{c^{(R)}}\right) = \mu_+ V^{(T)}\frac{\cos\psi^{(T)}}{c^{(T)}}. \tag{3.10}$$

From (3.8), (3.10) we compute the usual reflection coefficient

$$R = \left(\mu_-\frac{\cos\psi^{(I)}}{c^{(I)}} - \mu_+\frac{\cos\psi^{(T)}}{c^{(T)}}\right)\left(\mu_-\frac{\cos\psi^{(I)}}{c^{(I)}} + \mu_+\frac{\cos\psi^{(T)}}{c^{(T)}}\right)^{-1} \tag{3.11}$$

in terms of which

$$V^{(R)} = RV^{(I)}$$

$$V^{(T)} = (1+R)V^{(I)} \tag{3.12}$$

on $\bar{Z}$.

4 The beam superposition integral

We consider a beam leaving a point $x_0 \in R^2$ at angle θ to the x_1-axis. For convenience, we introduce the change of variables from arclength s to 'travel time' τ along the beam axis

$$\tau = \int_0^s \frac{ds'}{c}. \tag{4.1}$$

Equations (2.9) for the beam axis then become

$$\frac{\partial}{\partial\tau}\bar{x}(\tau,\theta) = c\,U_1(\tau,\theta) \tag{4.2a}$$

$$\frac{\partial}{\partial\tau}U_1(\tau,\theta) = -(\nabla c \cdot U_2)\,U_2(\tau,\theta). \tag{4.2b}$$

Comparing (2.10) with (4.1) we see that on the beam axis

$$\phi[\bar{x}(\tau,\theta)] = \tau. \tag{4.3}$$

Using $d/ds = c^{-1}\, d/d\tau$ in (2.16) yields

$$\frac{\partial}{\partial\tau}A(\tau,\theta) = cB$$

$$\frac{\partial}{\partial\tau}B(\tau,\theta) = -(U_2^T\nabla\nabla c U_2)A + (\nabla c \cdot U_1)B. \tag{4.4}$$

Initial conditions are that

$$\bar{x}(0,\theta) = x_0 \qquad A(0,\theta) = \epsilon$$

$$U_1(0,\theta) = (\cos\theta, \sin\theta)^T \qquad B(0,\theta) = 1$$

$$V(0,\theta) = 1/(4\pi i), \tag{4.5}$$

where the initial condition for V is a convenient normalization.

Let x_R be the position of a receiver. The field at x_R due to the beam at initial angle θ is denoted by $\bar{V}(\theta, x_R)\exp[i\omega\bar{\phi}(\theta;x_R)]$. We consider here the integral over θ of all such fields:

$$\bar{u}(x_R) = \int d\theta\; \bar{V}(\theta;x_R)\exp[i\omega\bar{\phi}(\theta;x_R)]. \tag{4.6}$$

Since $\bar{u}$ is a superposition of asymptotic solutions of the Helmholtz equation, as $\omega \to \infty$, $\bar{u}$ itself is an asymptotic solution as $\omega \to \infty$. We will show that it corresponds to a line source (a 2-D point source) at x_0. We consider first a medium without interfaces.

Let $\bar{n}(\theta;x_R)$ be the perpendicular distance from x_R to a point on the axis of beam θ and $\bar{\tau}(\theta;x_R)$ the corresponding travel time along the beam axis to this point. That is, we represent

$$x_R = \bar{x}[\bar{\tau}(\theta;x_R),\theta] + \bar{n}(\theta;x_R)\,U_2[\bar{\tau}(\theta;x_R),\theta]. \tag{4.7}$$

In the paraxial approximation

$$\bar{\phi}(\theta;x_R) = \bar{\tau} + \tfrac{1}{2}\bar{n}^2\frac{B}{Ac}, \tag{4.8}$$

where $A = A[\bar{\tau}(\theta;x_R),\theta]$, $c = c[\![\bar{x}[\bar{\tau}(\theta;x_R)]]\!]$, etc. In (4.6) we consider the superposition only of those beams θ for which $\bar{\tau}$ is positive. Their backward extensions, $\bar{\tau} < 0$, represent incoming solutions, and so fail to satisfy the Sommerfeld radiation condition. [This restriction has occasionally been overlooked in the literature (e.g. Červený *et al.* 1982, equations 47, 48)]. Since the beams are cut off at x_0, (4.6) solves the Helmholtz equation only in the exterior of a neighbourhood of this point.

With a view to the asymptotic analysis of (4.6), and in particular to the calculation of $\partial\bar{\phi}/\partial\theta$, we next compute derivatives with respect to θ of the various quantities. Since the beam axes correspond to ray-paths, the variational equations follow immediately from those of dynamic ray tracing. Thus

$$\frac{\partial\bar{x}}{\partial\theta} = A_1U_2$$

$$\frac{\partial U_1}{\partial\theta} = B_1U_2. \tag{4.9}$$

Here A_1 is the real-valued ray-tube area for a line source. A_1, B_1 satisfy (4.4) with the initial conditions (2.20).

Next, derivatives of $\bar{\tau}$, $\bar{n}$ may be computed by differentiating (4.7) and using (4.2), (4.9)

$$\frac{\partial}{\partial\theta}\bar{\tau}(\theta;x_R) = -\frac{\bar{n}B_1}{c[1+\bar{n}(\nabla c\cdot U_2/c)]} \tag{4.10a}$$

$$\frac{\partial}{\partial\theta}\bar{n}(\theta;x_R) = -A_1. \tag{4.10b}$$

Derivatives of $\bar{\phi}$ are computed from (4.8) using (4.10). The result simplifies upon use of the Wronskian relation (2.23).

$$\frac{\partial}{\partial\theta}\bar{\phi}(\theta;x_R) = \bar{n}(\theta;x_R)\,F(\theta;x_R) \tag{4.11a}$$

$$F(\theta;x_R) = \frac{\epsilon}{Ac_0[1+\bar{n}(\nabla c\cdot U_2/c)]} + \bar{n}\left[\frac{-(\nabla c/c\cdot U_2)A_1B}{cA[1+\bar{n}(\nabla c\cdot U_2/c)]} + \frac{1}{2}\frac{\partial}{\partial\theta}\frac{B}{Ac}\right], \tag{4.11b}$$

where $c_0 = c(x_0)$, and other quantities are evaluated at $\tau = \bar{\tau}$. In (4.11b) we need $\partial A/\partial\theta$, for instance, which we compute by the chain rule:

$$\frac{\partial}{\partial\theta}A[\bar{\tau}(\theta;x_R);\theta] = A_\tau\bar{\tau}_\theta + A_\theta.$$

A_τ, $\bar{\tau}_\theta$ are determined by (4.4), (4.10), while propagation equations for A_θ, B_θ can be obtained by differentiating (4.4) and using (4.9):

$$\frac{\partial}{\partial\tau}A_\theta = (\nabla c\cdot U_2)A_1B + cB_\theta$$

$$\frac{\partial}{\partial\tau}B_\theta = (2B_1A + A_1B)(U_1^T\,\nabla\nabla cU_2) - [U_2^T(\nabla\nabla\nabla c\cdot U_2)\,U_2]A_1A$$

$$+ (\nabla c\cdot U_2)B_1B - (U_2^T\nabla\nabla cU_2)A_\theta + (\nabla c\cdot U_1)B_\theta$$

$$A_\theta(0,\theta) = B_\theta(0,\theta) = 0. \tag{4.12}$$

Now, the behaviour of the integral (4.6) is in general determined by the saddle points, i.e. the zeros of expression (4.11a). Note that the zeros of $\bar{n}$ correspond to rays that hit the point x_R, the zeros of F do not. We assume temporarily that

(i) $\bar{n}(\theta;x_R) = 0$ at $\theta_1,\ldots,\theta_k$ which are on the real axis in the region of integration of (4.6).

(ii) $\theta_1,\ldots,\theta_k$ are 'sufficiently isolated' from each other.

(iii) There are no singularities of the integrand 'near' the path of integration.

(iv) The zeros of F are 'sufficiently far' from the path of integration.

The terms 'sufficiently isolated', 'near', etc., will be made more precise in subsequent sections, where we shall consider examples for which these assumptions are violated.

Then we compute, from (4.11), (4.10)

$$\frac{\partial^2\bar{\phi}}{\partial\theta^2}(\theta_j;x_R) = -\frac{A_1\epsilon}{Ac_0}. \tag{4.13}$$

From (2.19)

$$V(\theta_j;x_R) = -\frac{i}{4\pi}\left(\frac{\mu_0\,c^{(j)}\epsilon}{\mu^{(j)}c_0A^{(j)}}\right)^{1/2}, \tag{4.14}$$

where $A^{(j)} = A[\bar{\tau}(\theta_j;x_R);\theta_j]$, etc. The saddle-point method applied to (4.6) then yields

$$\bar{u}(x_R) \sim -\sum_{j=1}^{k}(-i)^{K_1}\frac{\exp(i\pi/4)}{\sqrt{8\pi(\omega/c^{(j)})}}\;\frac{\exp(i\omega\tau^{(j)})}{\sqrt{|A_1^{(j)}|}}\;\left(\frac{\mu_0}{\mu^{(j)}}\right)^{1/2}. \tag{4.15}$$

Here K_1 is the Keller–Maslov index, or the number of zeros of A_1 along the ray from x_0 to x_R (number of caustics). This interpretation of K_1 is obtained by considering the relation of the principal branch of $\sqrt{\epsilon/A}$ to that which varies continuously along the ray, and using the fact that for $A = A_1 + \epsilon A_2$

$$\frac{d}{ds}\arg A = \frac{d}{ds}\operatorname{Im}\log A = \operatorname{Im}\frac{B}{A} > 0$$

by (2.26), so that arg A increases along a ray and thus the zeros of A_1, A_2 interlace. Thus, (4.15) corresponds to the result of ordinary ray theory.

The following argument of Červený *et al.* (1982) suggests that (4.6) may be valid even when (4.15) fails. Consider a small circle of radius r_0 about x_0 within which the ray-field is regular, or, more specifically, suppose the medium is locally homogeneous, $c = c_0$ constant. For $|x_R| = r_0$, (4.15) reduces to

$$\bar{u}(x_R) \sim -\frac{\exp[i(\omega r_0/c_0)]}{\sqrt{8\pi(\omega r_0/c_0)}}\;\exp(i\pi/4) \sim -\frac{i}{4}H_0^{(1)}\left(\frac{\omega r_0}{c_0}\right),$$

where the Hankel function is the exact solution for a line source. Then $\bar{u}$ must be asymptotically a solution for the line source in the exterior, $|x_R| > r_0$ since it satisfies the equation in the exterior region, and also satisfies the appropriate boundary condition on $|x_R| = r_0$.

The above arguments are easily extended to include interfaces by including in (4.6) the sum of all reflected or refracted beams. Equation (4.14) must then be modified to include appropriate products of reflection and transmission coefficients via (3.12), and square roots of products of ratios of cosines and propagation speeds arising from the interface conditions for A, (3.6), (3.7). Again, the saddle-point method corresponds to naive ray theory, while the full integral (4.6) promises to handle arbitrary complications of the ray field.

Note that for (4.6) to be accurate its asymptotic behaviour should not depend on the complex parameter $\epsilon = \epsilon_1 + i\epsilon_2$ as long as $\epsilon_2 < 0$. However, in practice one is concerned with finite ω and then some values of ϵ are better than others. The 'optimal' choice suggested by Červený *et al.* (1982) is pure imaginary,

$$\epsilon_{opt} = -i|\delta| \tag{4.16}$$

with δ chosen to minimize the beam width at the receiver of the (assumed single) beam which hits the receiver. From (2.29), (2.26) this becomes

$$\delta = \frac{A_1}{A_2}, \tag{4.17}$$

as was derived by Červený *et al.* (1982). These authors called this choice 'optimal' because of its convenience in numerical calculations, although in later work they have investigated alternatives which produce better accuracy. Here we shall use this choice as a convenient benchmark.

5 The caustic boundary layer

In this section we consider the beam integral (4.6) near points x_R for which a critical point of ϕ is degenerate, i.e. near where not only $\phi_\theta = 0$ but also $\phi_{\theta\theta} = 0$. By (4.13) this happens when $A_1 = 0$, i.e. at a caustic.

It has often been noted that the beam integral is finite at a caustic, a distinct advantage over naive ray theory, which erroneously predicts an infinite amplitude as we see by setting $A_1 = 0$ in (4.15). The question now arises as to whether the beam integral is not only finite, like the true field, but whether it is an accurate representation of the true field asymptotically as $\omega \to \infty$. We shall demonstrate that this is not only for x_R in the neighbourhood of a smooth part of the caustic but also near cusps and other geometrical complexities. A typical example is the cusped caustic, generic in 2-D wave problems, which arises, for example, in the syncline problem to be described next.

The syncline

Let the x, y plane be occupied by two different media separated by the interface

$$y = f(x) \equiv d + \frac{h}{(1 + x^2/w^2)} > 0. \tag{5.1}$$

This configuration is meant to model a syncline.

Let the density and modulus be ρ_1, μ_1 in $y < f(x)$ and ρ_2, μ_2 in $y > f(x)$. Suppose a point source is situated at the origin. Then

$$\rho_1 u_{tt} - \nabla\cdot(\mu_1 \nabla u) = p(t)\,\delta(x)\,\delta(y), \qquad y < f(x), \tag{5.2}$$

$$\rho_2 u_{tt} - \nabla\cdot(\mu_2 \nabla)u = 0, \qquad y > f(x), \tag{5.3}$$

where u and μu_ν are continuous at $y = f(x)$

$$u = 0, \qquad t < 0 \tag{5.4}$$

Here $u_\nu \equiv \nu \cdot \nabla u$, where ν is the unit normal to the interface $y = f(x)$ with positive y component. Also, only outgoing waves exist for large $|x|$ or $|y|$. In the numerical calculations to be described later in this section, we chose

$$\mu_1 = \mu_2$$

$$c_1 = \sqrt{\frac{\mu_1}{\rho_1}} = 6000$$

$$c_2 = \sqrt{\frac{\mu_2}{\rho_2}} = 7000$$

$$d = 2000, \quad h = 100, \quad w = 100\sqrt{10} = 316.23, \tag{5.5}$$

where the units are feet and seconds.

Fig. 3 represents this structure. The specularly reflected rays are shown. Notice that they envelop a cusped curve (the caustic) which intersects the line $y = 0$ in two points. One can

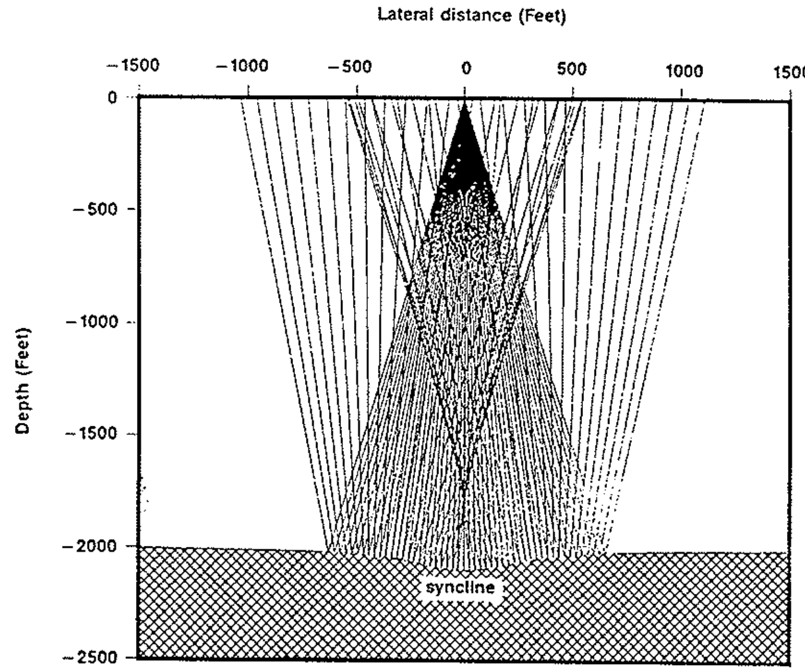

Figure 3. An angular sector of incident and reflected rays impinging on the syncline given by (5.1) with the parameters specified in (5.5). Notice the cusped caustic enveloped by the reflected rays.

easily check that three rays pass through each point within the cusped angular region bounded by the caustic and only one ray passes through each point outside this region. Thus naive ray theory would predict three arrivals within the cusp but only one outside it. We shall see that the beam superposition integral, the Kirchhoff integral, and finite difference calculations agree in predicting more than one arrival at points outside the cusp. The extra arrival not given by naive ray theory becomes smoother and smaller as the field point moves further from the caustic. This pulse can be associated with two complex (as opposed to real) rays which reach points outside the cusp. It can be understood also by way of Ludwig's (1966) theory for the smooth caustic, but naive ray theory misses this phenomenon altogether.

COALESCING CRITICAL POINTS

We shall now demonstrate that whereas naive ray theory is in principle incapable of yielding accurate results uniformly in a neighbourhood intersecting a caustic, the beam integral will, under fairly general conditions, yield accurate results uniformly near caustics of arbitrary complexity, e.g. cusped caustics.

In order to gain some understanding of the accuracy of the beam superposition integral on and near a caustic we notice first that the reflected field can be represented by a Kirchhoff integral over the reflecting interface $y = f(x)$ and that the caustic has no points in common with this interface. Secondly, we notice that asymptotically for large ω both the beam and the Kirchhoff integrals are of the standard form

$$I(\omega, \mathbf{x}) = \int_c g(\xi, \mathbf{x}) \exp [i\omega\phi(\xi, \mathbf{x})]\, d\xi \tag{5.6}$$

which has been studied extensively (see for instance Bleistein & Handelsman 1975). Theory tells us that for large ω only the behaviour of the integrand near the critical points ξ_c of ϕ defined by

$$\phi_\xi(\xi_c, \mathbf{x}) = 0 \tag{5.7}$$

need to be taken into account, and this is true whether or not the points ξ_c are well separated.

In order to compare the beam and the Kirchhoff integral we notice the following important facts:

(a) In both integrals the phase function $\phi(\xi, \mathbf{x})$ has as stationary values

$$\phi(\xi_c, \mathbf{x}), \tag{5.8}$$

the travel times along specularly reflected rays (i.e. rays for which the angle of reflection equals the angle of incidence).

(b) Except where $\phi_{\xi\xi}(\xi_c, \mathbf{x}) = 0$, the quantity

$$\frac{g(\xi_c, \mathbf{x})}{\sqrt{\phi_{\xi\xi}(\xi_c, \mathbf{x})}} \tag{5.9}$$

is the same for both integrals.

We shall now show that in a parameter range of $\mathbf{x}$ in which n critical points may coalesce or approach each other the two integrals agree asymptotically as $\omega \to \infty$. For this we draw upon Bleistein & Handelsman (1975), Section 9.3.

Consider $I(\omega, \mathbf{x})$ of (5.6). Suppose that in the parameter range of $\mathbf{x}$ under consideration, n critical points (ξ_p, $p = 1, \dots, n$,) may come together (in pairs or multiply) and that all other saddle points are well separated from these. Then we change variable of integration to $\zeta = \zeta(\xi)$ so that as a function of ζ the phase function is a polynomial of degree $n + 1$:

$$\begin{aligned}\phi(\xi, \mathbf{x}) &= \frac{1}{n+1}\zeta^{n+1} + \sum_{k=1}^{n-1} \frac{1}{k} a_k(\mathbf{x})\zeta^k + \phi_0(\mathbf{x}) \\ &= P(\zeta) + \phi_0(\mathbf{x}),\end{aligned} \tag{5.10}$$

where ϕ_0 and the $a_k(\mathbf{x})$ are to be determined so that

$$\phi_\xi(\xi, \mathbf{x}), \quad P'(\zeta) = \zeta^n + \sum_{k=1}^{n-1} a_k(\mathbf{x})\zeta^{k-1} \tag{5.11}$$

vanish simultaneously. Thus,

$$\zeta_p^n + \sum_{k=1}^{n-1} a_k(\mathbf{x})\zeta_p^{k-1} = 0, \qquad p = 1, \dots, n, \tag{5.12}$$

where $\zeta_p = \zeta(\xi_p)$. This ensures that the transformation $\zeta \to \zeta(\xi)$ is non-singular. We shall see that (modulo the ordering) the ζ_p are functions of the a_k, $k = 1, \dots, n-1$ (i.e. the vector $\mathbf{a}$).

There are in fact only $n - 1$ independent ζ_p since from (5.12)

$$\sum_{p=1}^{n} \zeta_p = 0.$$

Then

$$\frac{1}{n+1}\zeta_p^{n+1}(\mathbf{a}) + \sum_{k=1}^{n-1}\frac{1}{k} a_k\zeta_p^k(\mathbf{a}) + \phi_0 = \phi(\xi_p, \mathbf{x}), \qquad p = 1, \dots, n, \tag{5.13}$$

which is a system of n algebraic equations (which we assume is solvable). Then we may write

$$I(\omega, \mathbf{x}) = \exp(i\omega\phi_0)\int g[\xi(\zeta), \omega] \exp[i\omega P(\xi)]\frac{d\xi}{d\zeta}\, d\zeta. \tag{5.14}$$

In order to obtain the leading asymptotic term for large ω we set

$$g[\xi(\zeta), \omega]\frac{d\xi}{d\zeta} = \sum_{k=0}^{n-1} g_k\zeta^k + q(\zeta)P'(\zeta). \tag{5.15}$$

Here and in what follows primes denote derivatives. To determine the g_k we set $\zeta = \zeta_p$ in (5.15) to get

$$g(\xi_p, \omega)\frac{d\xi}{d\zeta}\bigg|_{\zeta_p} = \sum_{k=0}^{n-1} g_k\zeta_p^k, \qquad p = 1, \dots, n. \tag{5.16}$$

There is one small complication in calculating the left member of (5.16) which arises because

$$\frac{d\xi}{d\zeta} = \frac{P'(\zeta)}{\phi'[\xi(\zeta), \mathbf{x}]} \tag{5.17}$$

needs to be evaluated at ζ_p where both numerator and denominator vanish. But l'Hospital's rule gives

$$\lim_{\zeta\to\zeta_p}\frac{d\xi}{d\zeta} = \frac{P''(\zeta)}{\phi''[\xi(\zeta_p), \mathbf{x}]\; d\xi/d\zeta|_{\zeta=\zeta_p}} \tag{5.18}$$

which leads to

$$\frac{d\xi}{d\zeta}\bigg|_{\zeta=\zeta_p} = \left(\frac{P''(\zeta_p)}{\phi''[\xi(\zeta_p), \mathbf{x}]}\right)^{1/2}. \tag{5.19}$$

This is valid provided the denominator does not vanish.

The term $\Sigma\, g_k\zeta^k$ in (5.16) is in fact the Lagrange interpolating polynomial agreeing with $g\, d\xi/d\zeta$ at ζ_p, $p = 1, \dots, n$. On substituting (5.15) into (5.14) the term involving $P'(\zeta)$ may be integrated by parts and yields a term of lower order in $i\omega$. The terms involving the g_k are

$$\sum_{k=0}^{n-1} g_k \exp(i\omega\phi_0)\int\zeta^k \exp[i\omega P(\zeta)]\, d\zeta. \tag{5.20}$$

Here the integrals are (special) functions of the a_k which are in turn functions of the parameters $\mathbf{x}$ through equations (5.11) and (5.13). By (5.16) and (5.19) the g_k depend upon ϕ through P'' and ϕ'' and also on $g(\xi_p, \omega)$.

It is clear from this calculation that asymptotically for large ω the leading term is determined by $\phi(\xi_p, \mathbf{x})$ and $g(\xi_p, \mathbf{x})/[\phi''(\xi_p, \mathbf{x})]^{1/2}$. Thus, provided these quantities agree for the beam and the Kirchhoff integrals, and no other critical points approach the n critical points considered, the two integrals must agree asymptotically for large ω uniformly in $\mathbf{x}$.

[We remark that for parameter values $\mathbf{x}$ for which k critical points coalesce at ζ_c, ξ_c

$$\frac{d\xi}{d\zeta} = \left(\frac{p^{(k+1)}(\zeta_c)}{\phi^{(k+1)}(\xi_c, \mathbf{x})}\right)^{1/(k+1)}$$

and the $\phi^{(k+1)}(\xi_c, \mathbf{x})$ can be calculated by a limiting process from the $\phi''[\xi_p(\mathbf{x}), \mathbf{x}]$, where $\mathbf{x}$ is such that the $\xi_p(\mathbf{x})$ are distinct.]

THE KIRCHHOFF INTEGRAL

We next set up the Kirchhoff integral asymptotically for large ω. Let G be the Green function satisfying (2.1) with a non-homogeneous term representing a point source at (x_0, y_0):

$$\nabla \cdot (\mu \nabla G) + \rho\, \omega^2 G = \delta(x - x_0)\, \delta(y - y_0). \tag{5.21}$$

Then specializing to constant coefficients μ, ρ we have

$$G(\mathbf{x}, \mathbf{x}_0) = \frac{-i}{4\mu} H_0^{(1)}\left(\frac{\omega r}{c}\right), \qquad r = |\mathbf{x} - \mathbf{x}_0| \tag{5.22}$$

Since u satifies

$$\nabla \cdot (\mu \nabla u) + \rho\, \omega^2 u = 0, \tag{5.23}$$

we calculate

$$u(x_0, y_0) = \int_D \delta(x - x_0) \int \delta(y - y_0)\, u(x, y)\, dx\, dy$$

$$= \int_D [u\, \nabla \cdot (\mu \nabla G) - G\, \nabla \cdot (\mu \nabla u)]\, dx\, dy$$

$$= \int_{\partial D} \mu \left(u \frac{\partial G}{\partial \nu} - G \frac{\partial u}{\partial \nu}\right) ds, \tag{5.24}$$

where ∂D is a closed curve bounding the domain D. We may easily calculate u, $(\partial u/\partial \nu)\, G$, $(\partial G/\partial \nu)$ asymptotically to leading order as $\omega \to \infty$.

If ∂D is a reflecting interface and u_i is the incident field giving rise to reflected field u we find

$$u = R(\alpha) u_i \tag{5.25}$$

$$\frac{\partial u}{\partial \nu} = -R(\alpha) \frac{\partial u_i}{\partial \nu} = -R \frac{i\omega}{c} \cos \alpha\, u_i \tag{5.26}$$

to leading order in $i\omega$, where α is the angle between the incident ray and the normal while $R(\alpha)$ is the reflection coefficient given in (3.11).

Replacing $H_0^{(1)}$ in (5.22) by its asymptotic approximation

$$H_0^{(1)}\left(\omega \frac{r}{c}\right) = \left(\frac{2c}{\pi \omega r}\right)^{1/2} \exp\left[i\left(\frac{\omega r}{c} - \frac{\pi}{4}\right)\right] \tag{5.27}$$

we obtain to leading order in ω

$$\frac{\partial G}{\partial n} = i \frac{\omega}{\mu} \frac{\partial}{\partial n}\left(\frac{r}{c}\right) \left(\frac{2c}{\pi \omega r}\right)^{1/2} \exp\left[i\left(\frac{\omega r}{c} - \frac{\pi}{4}\right)\right]$$

$$= \frac{i\omega}{c} \cos \psi\, G, \tag{5.28}$$

where ψ is the angle between the normal to ∂D and the ray from $\mathbf{x}_0$ to $\mathbf{x}$ on ∂D. Finally, to leading order (5.24) becomes

$$u(x_0, y_0) = \int_{\partial D} \frac{i\omega\mu}{c} R(\alpha)\, u_i G(\cos\psi + \cos\alpha)\, ds$$

$$= \frac{1}{16} \int_{\partial D} \frac{-i\omega}{\mu c} R(\alpha)(\cos\psi + \cos\alpha) \left(\frac{2c}{\pi\omega r_0}\right)^{1/2} \left(\frac{2c}{\pi \omega r}\right)^{1/2}$$

$$\exp\left[i\left(\frac{\omega}{c}(r + r_0) - \frac{\pi}{2}\right)\right] ds$$

$$= \frac{-1}{8\pi} \int_{\partial D} \frac{R(\alpha)(\cos\psi + \cos\alpha)}{\mu (r_0 r)^{1/2}} \exp\left(i \frac{\omega}{c}(r_0 + r)\right) ds \tag{5.29}$$

where we have used the fact that $u_i(\mathbf{x}) = G(\mathbf{x}, 0)$, given in (5.22), and set $r_0 = |\mathbf{x}_0|$. This integral may now be evaluated asymptotically to give the same result as naive ray theory when certain critical points are distinct, each critical point of $r + r_0$ corresponding to a distinct ray. The stationary points of $r_0 + r$ are just the points of reflection of specularly reflected rays which pass through the receiver. The stationary values of $(r_0 + r)/c$ are just the total travel time along the incident and reflected segments of the ray path. When evaluated at a critical point, the factor outside the exponential in (5.29) combines with $[\![[d^2(r_0 + r)]/ds^2]\!]^{-1/2}$ to form precisely the amplitude predicted by ray theory.

When the field point is near a caustic the critical points in (5.29) approach each other and both naive ray theory and the naive asymptotic evaluation of (5.29) break down. However, (5.29) remains asymptotically an accurate representation of the reflected field and, because of the structural similarity between the Kirchhoff integral and the beam integral, the latter also faithfully represents the field uniformly as $\mathbf{x}$ varies near a caustic. Thus the beam superposition integral accurately represents the field uniformly in the vicinity of a caustic of arbitrary complexity asymptotically as $\omega \to \infty$ provided that the only critical points which cluster together correspond to specularly reflected rays. But as we shall see later it can happen that non-geometrical critical points of ϕ given by zeros of F in (4.11a) may approach the geometrical ones and cause the beam integral to be inaccurate.

NUMERICAL CALCULATIONS FOR THE SYNCLINE

In order to evaluate the effectiveness of the beam integral method and to compare it with naive ray theory we calculated the reflected field in the syncline problem in four different ways in the caustic region:

(a) simulated the problem with a finite difference time-dependent wave-equation solver (fourth order accurate in space, second in time, see Appendix B for details);
(b) evaluated a Kirchhoff integral representation of the reflected field in the time domain;
(c) evaluated the formulae of naive ray theory;
(d) performed the beam integral numerically for Červený's optimal ϵ_{opt} of (4.16);
(e) performed the beam integral numerically for $\epsilon = -2687 - 265i$.

The purpose of (a) and (b) was to provide 'exact' solutions against which the accuracy of (c), (d) and (e) could be judged. In the absence of an analytic solution it was thought prudent to calculate the (nominally) exact solution in two completely independent ways, the agreement of which provides strong corroboration of the accuracy of each.

In these calculations we were not concerned with speed of calculation or the effect of coarseness of stepsize in the numerical integrations or in the finite-difference calculation. In each case sufficiently fine grids were imposed that we were essentially performing the calculations exactly. Thus we are comparing *mathematical methods* rather than approximate implementations of those methods.

With the syncline interface given by (5.1) and parameters as specified in (5.5) the caustic cuts the line $x = 0$ at approximately $x = \pm 506$. The cusp of the caustic lies at $x = 0$, $y = 1816$. In order to illustrate the various methods in the neighbourhood of the caustic we took various receiver positions on $y = 0$ with x varying from 0 past $x = 500$ to 3000. It is remarkable how broad the so-called caustic boundary layer is. Of course this is a function of the pulse width which in our calculations we may take to be about 0.1 s corresponding to a pulse length in space of 600 ft, which is comparable with the width of the syncline. The wavelength corresponding to the centre frequency is somewhat less than around 300 ft.

The time-dependent source had the form of (5.2), where $p(t)$ is the wavelet:

$$p(t) = (t - t_0)\left\{\exp\left[-2\left(\frac{t - t_0}{t_1}\right)^2\right] - \exp\left[-2\left(\frac{t_0}{t_1}\right)^2\right]\right\}, \qquad 0 < t < 2t_0$$

$$= 0 \qquad t < 0, t > 2t_0 \tag{5.30}$$

with $t_0 = 0.0285$, $t_1 = 0.019$.

The shape of the travelling pulse launched by this source is a one-half integral $(I_{1/2}p)(t)$ of $p(t)$, and according to naive ray theory it is this pulse shape or its Hilbert transform $(I_{1/2}P)'(t)$ which is carried by each geometrical arrival.

Three specularly reflected rays arrive at each point within the cusp of the caustic and in particular at receiver locations for $0 < x < 500$, $y = 0$. Actually the arrival times associated with two of these coincide at $x = 0$ and the arrival times for other pairs coincide on the caustic $x \sim \pm 506$. Only one specularly reflected ray arrives at each point outside the cusp (at our receiver locations for $|x| > 506$).

The numerical results (Figs 4–9) at first sight seem to be at variance with this. For $0 < x < 250$ there appears to be only one arrival for all five methods of computation. By $x = 500$ the pulse appears to be a superposition of two arrivals. Beyond $x = 506$ the ray theory gives just the one arrival but the other four agree in giving two arrivals, which we easily see well separated in time for $x = 2000$. The second pulse is small and gets smaller as x increases until it is quite insignificant for $x = 3000$.

On tracing these pulses as x decreases from 2000 towards 500 we see the second pulse becoming larger and closer to the large first arrival. While naive ray theory does not explain

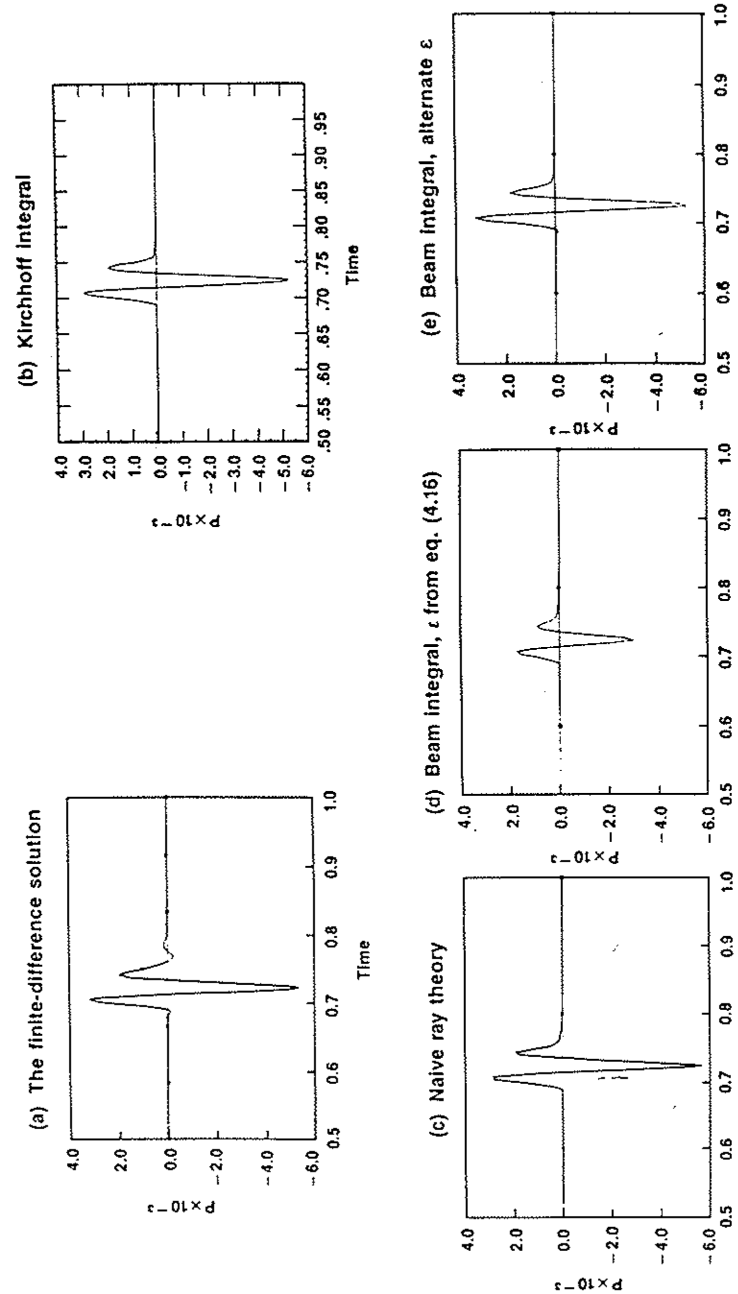

Figure 4. For comparison we plot the seismograms computed in five different ways for a receiver located at $x = 0, y = 0$.

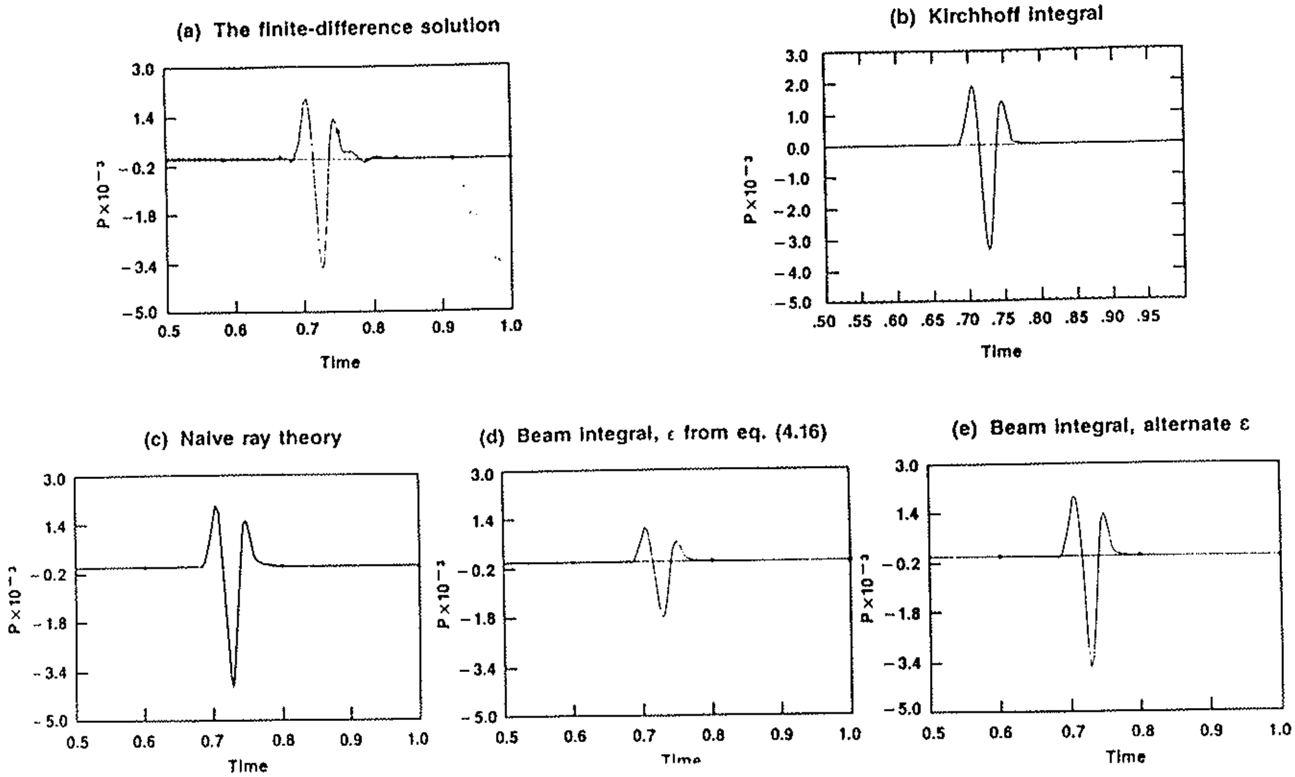

Figure 5. Same as Fig. 4 for receiver at $x = 250, y = 0$.

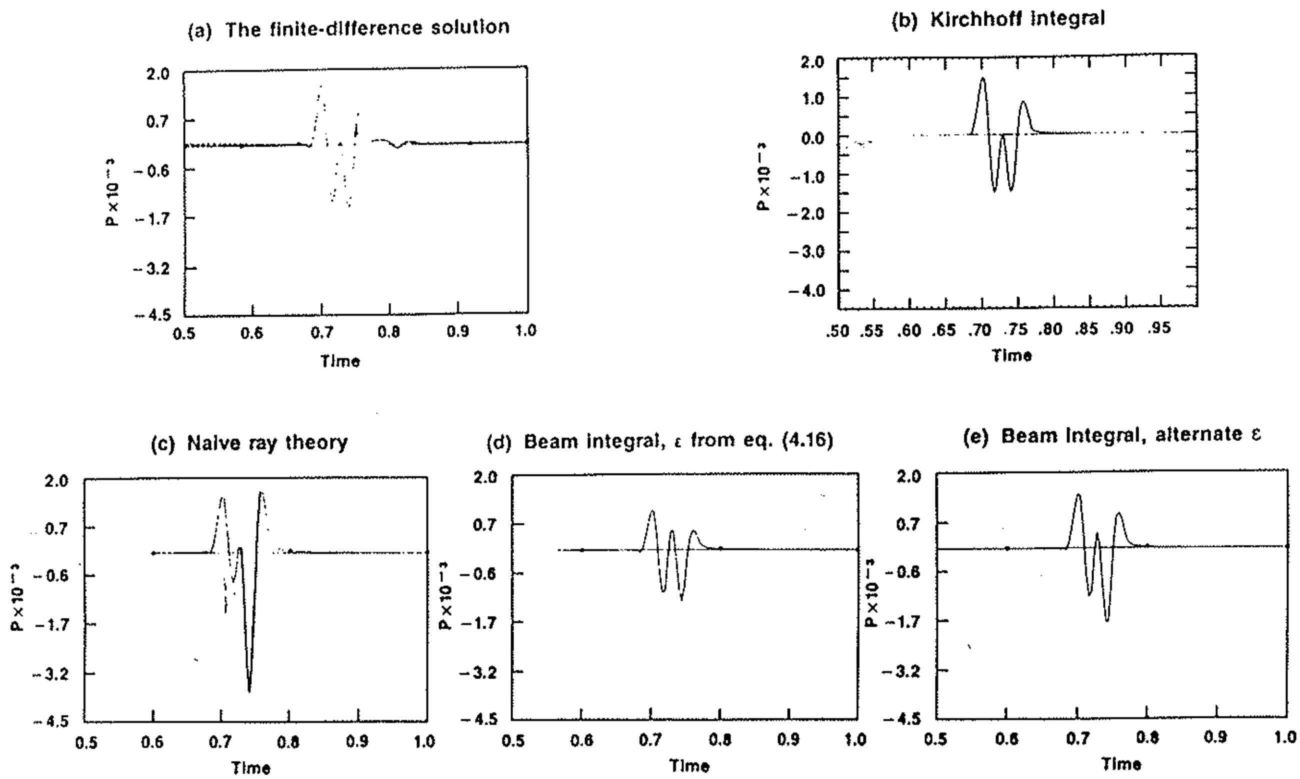

Figure 6. Same as Fig. 4 for receiver at $x = 500, y = 0$.

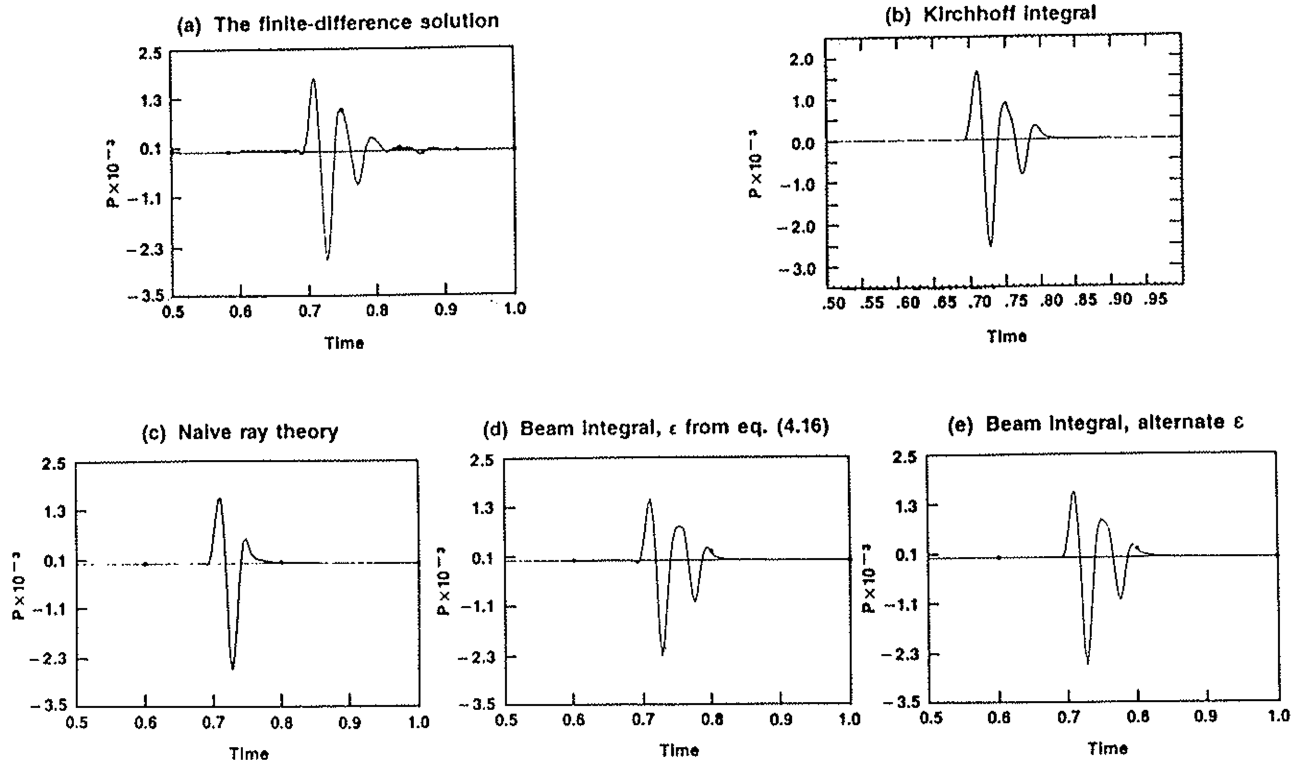

Figure 7. Same as Fig. 4 for receiver at $x = 1000, y = 0$.

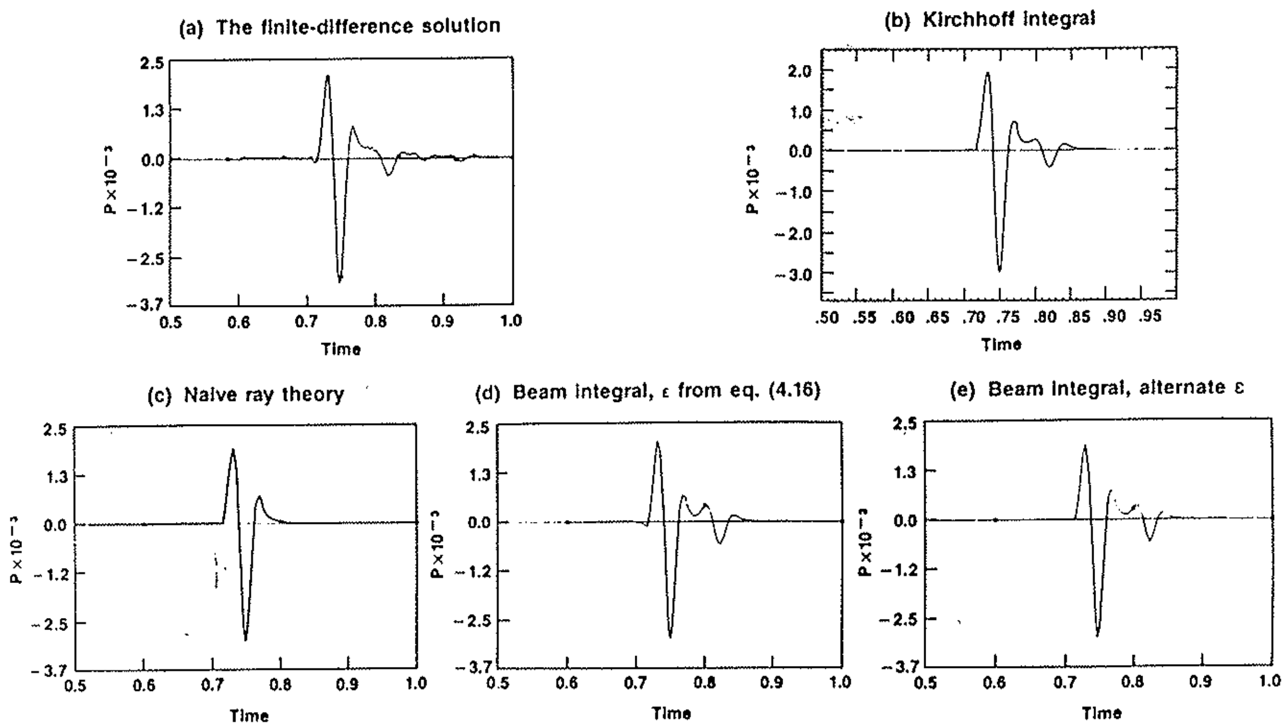

Figure 8. Same as Fig. 4 for receiver at $x = 1500, y = 0$.

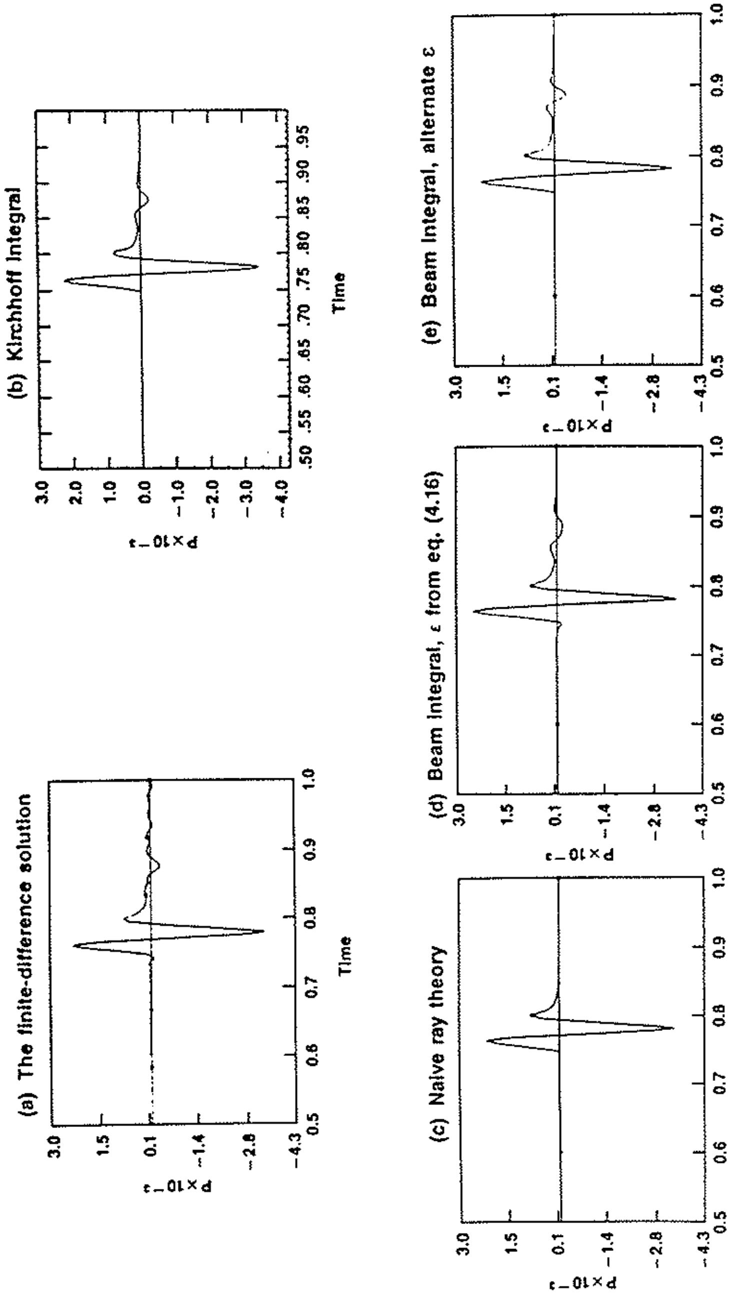

Figure 9. Same as Fig. 4 for receiver at $x = 2000, y = 0$.

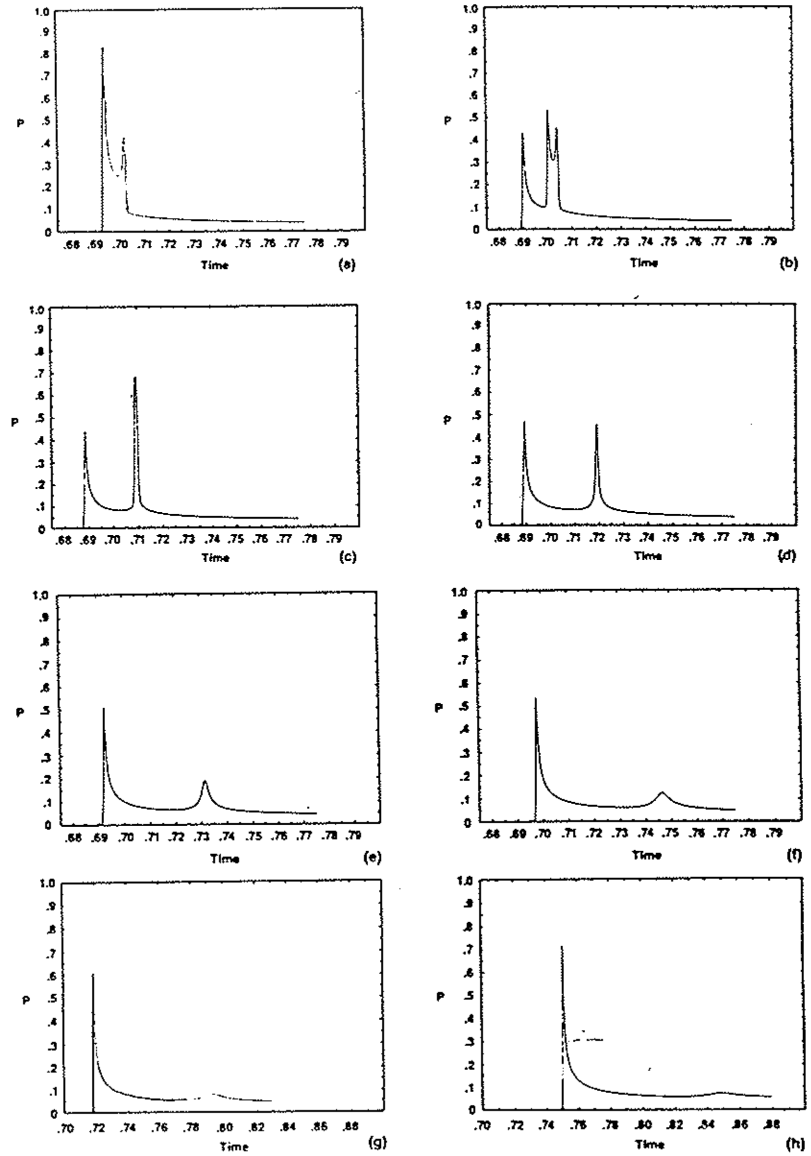

Figure 10. The Green function (impulse response) for an impulsive source at $x = 0, y = 0$ and receivers at: (a) $x = 0, y = 0$; (b) $x = 200, y = 0$; (c) $x = 400, y = 0$; (d) $x = 600, y = 0$; (e) $x = 800, y = 0$; (f) $x = 1000, y = 0$; (g) $x = 1500, y = 0$; (h) $x = 2000, y = 0$.

these results Ludwig's related theory of the smooth caustic does explain them especially when we take into account the great length of our pulse. The fact that only one pulse is apparent for $0 < x < 250$ is not in contradiction with the three ray arrivals. It turns out that the differences in arrival times of the separate rays are so small and so much shorter than the pulse length that three arrivals are superposed almost in phase and so appear as one, although there is some modification of pulse shape owing to one arrival being the Hilbert transform of the other two. As x increases to 500 near where the caustic crosses $y = 0$, one arrival (the first) separates more and more from the other two, which coincide on the caustic. Beyond $x = 506$ the receiver is on the 'dark' side of the caustic. Here in addition to the one specular ray Ludwig's theory predicts a smooth diffuse pulse in the impulse response which may be regarded as the contribution from two complex (non-real) rays which are analytic continuations to the dark side of the caustic of the two real rays mentioned above which coincide on the caustic. Our computations should then yield a time convolution of this with the pulse shape. Because the length of our pulse is so great the diffuse pulse in the impulse response is much shorter and, for the purpose of the convolution, it behaves like a δ-function. It therefore produces a late arrival with the pulse shape p.

To verify this interpretation the Kirchhoff integral representation of the impulse response was calculated for the same receiver positions. It is clear from Fig. 10 that the diffuse pulse on the dark side of the caustic may be regarded as an extension to the dark side of the two extra arrivals present on the illuminated side.

Thus we have not only computed the field by two different, potentially accurate methods (a) and (b), which agree, but we have explained their slightly paradoxical results heuristically. Thus we have considerable faith in their accuracy. We may now examine in what ways the ray and beam calculations deviate from these and from each other.

THE CUSPED REGION $0 < x < 250$ (FIGS 4, 5)

Here methods (a), (b), (c) are in good agreement but the beam integrals (d) using Červený *et al.*'s optimal ϵ yields the correct pulse shape with too small an amplitude. However, by using a different value of ϵ (e) (see Section 7) the beam integral solution can be made to agree well with (a), (b), (c).

THE CUSPED REGION NEAR THE CAUSTIC $x = 506$ (FIG. 6)

Here methods (a) and (b) agree and are taken to be exact. Method (c), ray theory, yields inaccurate amplitudes in the latter part of the pulse. This is associated with the erroneous infinite amplitudes predicted by naive ray theory at the nearby caustic for the nearly simultaneous second and third ray arrivals. The beam integral (d) with Červený *et al.*'s optimal ϵ errs in a different way but again the beam integral with suitably chosen ϵ(e) yields a quite accurate result.

BEYOND THE CAUSTIC $x > 500$ (FIGS 7–9)

Here the exact pulse given by (a) and (b) is quite complicated. Naive ray theory with its single ray arrival is incapable of predicting a pulse of this complexity and is quite inaccurate until $x \sim 3000$ where the single ray captured by naive ray theory does, in fact, dominate the solution. The beam integral, especially with the modified ϵ, does capture the complexities of the pulse and yields a quite accurate solution.

As x increases beyond about 1250 the latter part of the pulse detaches itself more and more from the earlier part and the signal essentially splits into two arrivals. The first arrival is well predicted by ray theory. The second pulse is missed altogether by ray theory but the beam integral captures the whole pulse sequence. Again modifying ϵ from Červený *et al.*'s optimum to a suitable value improves its accuracy. We notice that for $2000 < x < 3000$ the finite-difference scheme seems to predict a slightly early arrival time for the second pulse. By $x = 3000$ this second pulse has become quite small and we seem to be at the outer limit of the caustic boundary layer.

SUMMARY OF RESULTS ON THE EFFECTIVENESS OF THE BEAM INTEGRAL METHOD AND OF NAIVE RAY THEORY IN THE CAUSTIC BOUNDARY LAYER

Our numerical computations bear out our theoretical claim that the beam integral is capable of yielding an accurate solution near a caustic of arbitrary complexity, provided that no other singularities of the integrand or critical points of the phase come near those critical points associated with the geometrical (specularly reflected) rays. As we shall see, the fact that some values of ϵ in the beam integral yield better results than others can be well explained by the shifting of non-geometrical critical points [zeros of F in (4.11b)] away from the path of integration in (4.6).

6 Reflections from a circular cylinder: effects of large curvature

In this section we illustrate, for the case of a circular cylinder, how the beam superposition solution can deteriorate when the problem involves large interface curvature. This phenomenon is associated with a dependence of the beam integral on the 'free' beam parameter ϵ. An analysis of this dependence yields the range of ϵ-values for which the deterioration is minimized. In contrast to previous authors, who have taken ϵ on the negative imaginary axis, our values are nearly real.

The inaccuracy is due to the presence of spurious points, which are complex zeros of the second factor F in (4.11a). The zeros of the first factor $\bar{n}$ correspond to beams whose axes hit the receiver. When we bear in mind that such beam axes are specularly reflected rays joining the source to the cylinder and then to the receiver we see that these zeros give meaningful contributions according to ray theory. From Section 5, this class of 'true' saddles includes complex-valued roots of $\bar{n}$ corresponding, on the dark sides of caustics, to analytic continuations of rays from the bright side. In contrast, the roots of $F = 0$ are artefacts of the method, and their position and influence on the beam integral can be strong functions of ϵ.

For propagation through piece-wise homogeneous media, we see from (4.11b) that F has the form

$$F(\theta) = \frac{\epsilon}{Ac} + \frac{1}{2}\frac{\bar{n}}{c}\frac{\partial}{\partial\theta}(K), \tag{6.1}$$

where $K = B/A$ is the complex-valued wavefront curvature. Now a root, θ_+, of $F = 0$ will have only exponentially small influence on the beam integral unless $\mathrm{Im}\,\phi(\theta_+)$ is near zero. From (4.8) this can occur, for θ_+ near the real axis, only when $\bar{n}$ is small, since then $\bar{n}, \bar{\tau}$ are nearly real but B/A is not. That is, influential spurious saddles near the real axis are close to true saddles. Thus they will not produce spurious arrivals. Rather, they will coalesce with the true arrivals to produce a signal described by the wrong canonical integrals giving distorted pulse shapes and amplitudes but at approximately the right arrival time.

Now since $\bar{n}$ is small at θ_+, while ϵ/A is not, it follows from (6.1) that $(\partial/\partial\theta)K$ is large. That is, the wavefront curvature must vary rapidly as a function of θ for spurious saddles to occur.

Equation (6.1) may be simplified for propagation through a homogeneous medium, and reflection from a single interface. For the beam leaving the source at angle θ, let r_1 be the distance from source to the point where the beam axis intersects the interface (see Fig. 11 for the case of the cylinder). Let r_2 be distance to the point of closest approach to the receiver, and let ψ be the angle of incidence, and a the radius of curvature at the point on the interface. We can then use (2.16), (3.6), (3.7) to obtain

$$-A = r_1 + \epsilon + r_2\left(1 + \frac{2(r_1+\epsilon)}{a\cos\psi}\right)$$

$$-B = 1 + \frac{2(r_1+\epsilon)}{a\cos\psi}. \tag{6.2}$$

The equation $F = 0$ now follows from (2.15), (6.1) and (6.2) as

$$\bar{n}\frac{\partial}{\partial\theta}\frac{2}{a\cos\psi} - \frac{1}{(r_1+\epsilon)^2}\frac{\partial}{\partial\theta}r_1 - \left(\frac{1}{(r_1+\epsilon)} + \frac{2}{a\cos\psi}\right)^2\frac{\partial}{\partial\theta}r_2$$

$$= \frac{2\epsilon}{(r_1+\epsilon)}\left(1 + \frac{r_2}{(r_1+\epsilon)} + \frac{2r_2}{a\cos\psi}\right). \tag{6.3}$$

We next derive an expression for the beam solution for reflection from the top of a circular cylinder of radius a. Let r_0, r be distances from the centre of the cylinder to, respectively, source and receiver, and let θ_0 be the central angle, as in Fig. 11. Let c_0, c_1 be speeds, respectively, outside and inside the cylinder, and let $\gamma = c_1/c_0$. We take $\rho = 1$, so that the field and its normal derivative are continuous across the interface. Let $D = r_0 - a$ be the distance from source to interface. We define

$$\eta = \frac{r_0}{a} = 1 + \frac{D}{a}. \tag{6.4}$$

Reference to Fig. 11 yields, for the reflection angle ψ,

$$\sin\psi = \eta\sin\theta, \tag{6.5}$$

also

$$r_1 = r_0\cos\theta - a\cos\psi$$

$$r_2 = r\cos(2\psi - \theta - \theta_0) - a\cos\psi$$

$$\bar{n} = r\sin(2\psi - \theta - \theta_0) - a\sin\psi. \tag{6.6}$$

The angle of refraction ψ_1, is determined by (3.4), and the reflection coefficient, R, by (3.11). The beam superposition integral is then given, for $k = \omega/c_0$, by

$$U_B = \frac{i}{4\pi}\int_{|\sin\theta| < a/r_0} R(\epsilon/A)^{1/2}\exp(ik\tilde{\phi})\,d\theta, \tag{6.7a}$$

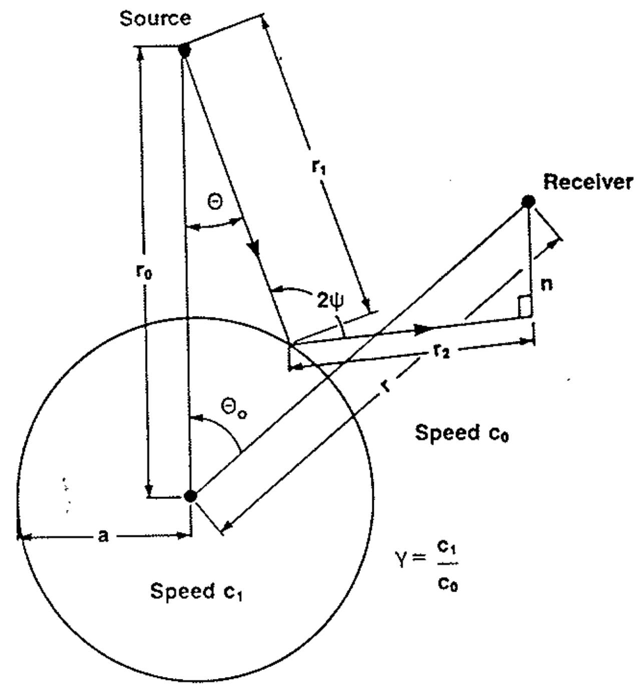

Figure 11. Reflections from a circular cylinder by Gaussian beams. Beam paths to closest approach, distance n, to receiver.

where

$$\tilde{\phi} = r_1 + r_2 + \tfrac{1}{2}\bar{n}^2 B/A \quad \text{and} \quad r_2 > 0. \tag{6.7b}$$

The restrictions on the integral in (6.7a) specify that the beam hits the cylinder, and is reflected back in the direction of the receiver.

The beam, $\hat{\theta}$, that hits the receiver, is the solution of $\bar{n} = 0$, where $\bar{n}$ given in (6.5). Since $A = A_1 + \epsilon A_2$, the real ray-tube areas, A_1, A_2 for this beam may be obtained from (6.6). The value of ϵ suggested by Červený *et al.* (1982) may then be obtained from the values $\hat{\psi}$, $\hat{r}_1$, $\hat{r}_2$ for this beam as

$$\epsilon_c = -i\delta$$

$$\delta = \frac{\hat{A}_1}{\hat{A}_2} = \frac{(a\cos\hat{\psi}\,[\hat{r}_1 + \hat{r}_2] + 2\hat{r}_1\hat{r}_2)}{(a\cos\hat{\psi} + 2\hat{r}_2)} \tag{6.8}$$

Similar expressions may be obtained for multiple reflections within the cylinder, but we omit the details.

An exact solution is obtained by separation of variables, see e.g. Morse & Feshbach

(1953). The incident field is given by (5.22), where x_0 is the source. The reflected field is

$$u_{ref} = -\frac{i}{4} \sum_{m=0}^{\infty} \beta_m H_m^{(1)}(kr_0) H_m(kr) \cos m\theta \tag{6.9}$$

$$\beta_m = \alpha_m \frac{J_m(ka) J_m'(ka/\gamma) - \gamma J_m'(ka) J_m(ka/\gamma)}{H_m^{(1)}(ka) J_m'(ka/\gamma) - \gamma H_m^{(1)\prime}(ka) J_m(ka/\gamma)}.$$

$$\alpha_m = \begin{cases} 1, & \text{for } m = 0 \\ 2, & \text{for } m \neq 0. \end{cases}$$

Fig. 12(a–d) are for the case $D = 1000$ ft, $a = 500$ ft, $c_0 = 6000$ ft s^{-1}, $c_1 = 7000$ ft s^{-1}, and coincident source and receiver. Shown are reflections in the time domain for the pulse, given by equation (5.31) for which the peak frequency is at 20 Hz.

Fig. 12(a) is the exact solution, computed by equation (6.9) and brought into the time domain by fast Fourier transform. Fig. 12(b) is the beam solution, for which we have computed only primary arrivals from the top and the bottom of the cylinder, for the choice $\epsilon = \epsilon_c$ given by (6.8) and for coincident source and receiver, $\theta_c = 0, r_0 = r$. Thus,

$$\epsilon_c = -i\delta$$

$$\delta = \frac{2D(D+a)}{(2D+a)}. \tag{6.10}$$

There is a significant degradation of the beam solution involving a decrease in amplitude and a change in pulse shape, e.g. the new pulse has a leading negative peak not in the exact

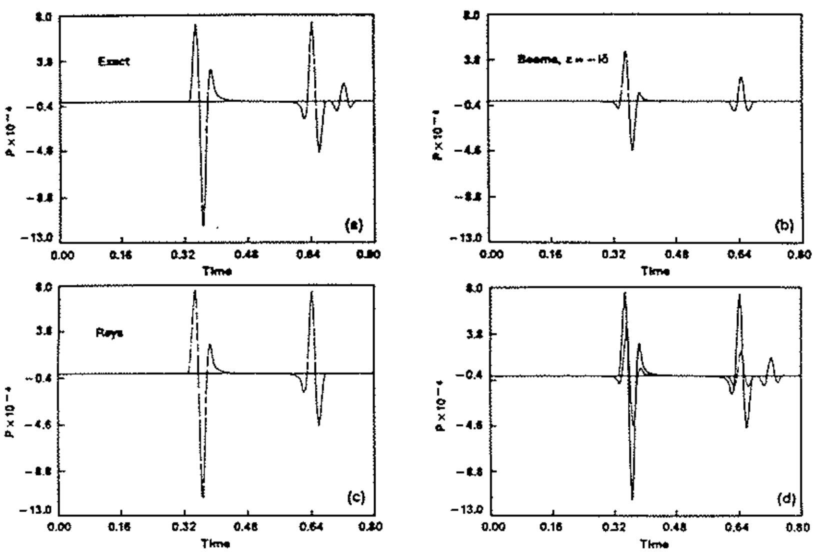

Figure 12. Comparison of solutions for a circular cylinder of radius 500 ft at a depth of 1000 ft, with coincident source and receiver. The ray and beam solutions contain only primary reflections from top and bottom of the cylinder. Although the arrival times are correct for the beam solution, there is a discrepancy in pulse shape as well as amplitude. (a) 'Exact' solution obtained by separation of variables; (b) beams, with $\epsilon = -i\delta$ from Equation (4.16); (c) ray theory; (d) superposition of solutions.

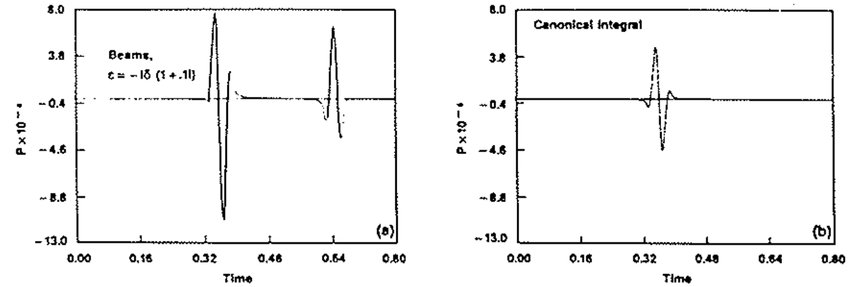

Figure 13. Interpretation of the results of Fig. 12 in terms of spurious saddle points. (a) The beam solution with $\epsilon = -\delta(1 + 0.1i)$ decreases the effect of the spurious saddles, producing agreement with Fig. 12(a), (b); (b) the canonical integral for the coalescence of two spurious saddles with the true saddle produces agreement with Fig. 12(b) for reflection from top of cylinder.

solution. Note that this discrepancy occurs even though the large parameters governing the asymptotic expansion are $kD \approx 20, ka \approx 10$. By contrast, the ray-theory solution (Fig. 12c), is indistinguishable from the exact for the two primary reflections computed. In Fig. 12(d) we see the arrival times predicted by the beams are reasonable to within an uncertainty due to the altered pulse shape.

To obtain an approximate expression for the spurious saddles, equations (6.4), (6.5) are expanded as Taylor series in θ, and the resulting expressions put into (6.2). If only $0(\theta^2)$ terms are retained, the resulting quadratic equation may be solved for two spurious saddles, $\theta_+, \theta_- = -\theta_+$, where

$$\theta_+ = \frac{1}{\eta}\left[\!\left[\frac{\epsilon}{a}\left[2\eta^2 + 2\left(\frac{\epsilon}{a} - 1\right)\eta - \frac{\epsilon}{a}\right]\right]\!\right]^{1/2}$$
$$\times \left[\!\left[(\eta - 1)\left[(4\eta^2 - 5\eta + 1)\left(2\eta + 2\frac{\epsilon}{a} - 1\right)^2 - 2\eta\left(\eta - 1 + \frac{\epsilon}{a}\right) - \eta + 1\right]\right]\!\right]^{-1/2} \tag{6.11}$$

In deriving (6.11) we have neglected $0(\theta^2)$ terms on the rhs of (6.2), which are higher order in η.

For the case depicted in Fig. 12, equation (6.11) yields $\theta_+ = 0.0414 - 0.0178i$, in good agreement with the result $\theta_+ = 0.0411 - 0.0171i$ obtained by means of an iterative complex root-finder based on the exact equation for $F(\theta)$. Similar agreement was found for a range of parameter values provided η, here equal to 3, was relatively large.

A more comprehensive picture of the roots in the complex θ-plane is afforded by the argument principle

$$\frac{1}{2\pi i}\int_{|\theta| = \theta_m} \frac{F'(\theta)}{F(\theta)}\, d\theta = (\text{number of spurious saddles}) - (\text{number of poles}) \quad \text{for } |\theta| < \theta_m. \tag{6.12}$$

The poles referred to are zeros in the complex θ-plane, of A, and correspond to caustics of complex rays. From (6.7) they are essential singularities in the beam integrand.

Use of (6.12) in the present example indicated two saddles for $|\theta_m|$ between 0.044 and 0.045, and no other contributions to (6.14) until four poles were encountered for $|\theta_m| = 0.26$.

We next approximate $\hat\phi(\theta) - \hat\phi(0)$, as a quadratic function of θ^2. Using $\hat\phi' = 0$ at $\theta = 0$, $\pm\theta_+$, and the expression for $\hat\phi''(0)$ given by (4.13), the result is

$$\hat\phi(\theta) - \hat\phi(0) \approx \frac{-\epsilon\delta}{4(\epsilon+\delta)\theta_+^2}(\theta^4 - 2\theta_+^2\theta^2). \tag{6.13}$$

Use of (6.13) for the present example, with θ_+ approximated by (6.11) yielded $\hat\phi(\theta_+) - \hat\phi(0) = 0.0009 + 0.04201i$, in reasonable agreement with the exact value, $0.0058 \pm 0.4249i$. Thus, fairly accurate computations can be done by Taylor series.

A cruder, but more illuminating approximation to θ_+ is obtained by expansion of (6.11) for large η, retaining only leading terms, and taking $\epsilon/a = O(\eta)$.

$$\theta_+ \approx \frac{1}{4\eta^2}\frac{\sqrt{2\epsilon}}{(\epsilon+\delta)} \tag{6.14}$$

The influence on the beam integral is obtained by using (6.14) in (6.13) and setting $\theta = \theta_+$

$$\hat\phi(\theta_+) - \hat\phi(0) \approx \frac{-\epsilon^2\delta}{32\eta^4(\epsilon+\delta)^2}. \tag{6.15}$$

Thus from (6.14) and (6.15), θ_+ may be moved away from the real axis, and its influence $|\exp[\![ik[\hat\phi(\theta_+) - \hat\phi(0)]]\!]|$ exponentially reduced by taking ϵ near $-\delta$, in the lower half-plane.

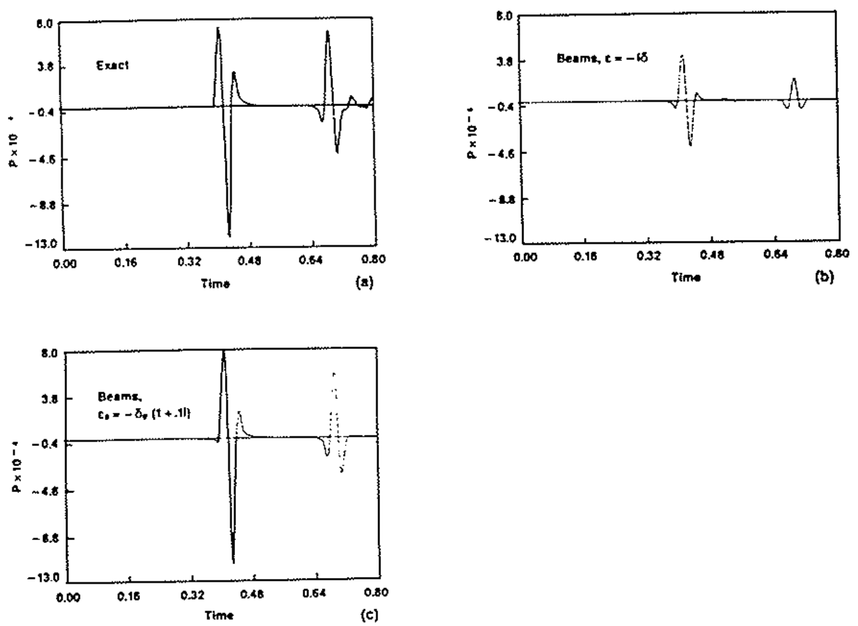

Figure 14. Comparison of solutions for a cylinder of radius 500 and 1000 ft below the source, for a receiver at 1000 ft offset. (a) 'Exact' solution obtained by separation of variables; (b) the beam solution, with $\epsilon = -i\delta$, is inaccurate as at zero offset (Fig. 12b); (c) the beam solution is considerably improved by the choice $\epsilon = -\delta_0(1 + 0.1i)$, identical to that used at zero offset.

Fig. 13(a) shows how accuracy in the beam integral is restored by the choice $\epsilon = -\delta(1 + 0.1i)$. Fig. 13(b) shows how the results of the beam solution, for $\epsilon = \epsilon_c = -i\delta$ (Fig. 12b) are accurately predicted by the canonical integrals for the coalescence of three saddles, as discussed in Section 5. The inputs to this calculation were only θ_+, and the values of $\tilde\phi$, $R(\epsilon/\tilde\phi'')^{1/2}$ at $\theta = 0, \pm\theta_+$.

Fig. 14 shows the return for a receiver at a 1000 ft offset, when the cylinder is directly under the source. For $\epsilon = \epsilon_c = -i\delta$, with δ recomputed for this receiver, the beam integral (Fig. 14b) is in disagreement with the exact solution (Fig. 14a). Accuracy is restored to the beam solution by using the identical value of ϵ which worked at zero offset, i.e. that from Fig. 13(a).

Fig. 15 shows a more extreme case, for which $\eta = 6$, $D = 2500$ ft, $a = 500$ ft.

It seems physically reasonable to surmise that the beam integral is accurate if and only if the beam width at the interface is much smaller than the radius of curvature of the interface. This condition, however, is neither necessary nor sufficient. Since the rays are quite accurate for frequencies higher than 20 Hz, we compare only primary reflections from the top of the cylinder by comparing the beams and the rays in the frequency domain. Thus for $D = 1000$ ft, $a = 500$ ft, $\epsilon = \epsilon_c$ and a frequency of 20 Hz the beam width at the interface is 311 ft, and we may suspect that this is the source of the inaccuracy. However, discrepancies of over 37 per cent are found to persist at 1000 Hz, when the beam width is only 44 ft. Since $|\exp[ik\hat\phi(\theta_+)]| = 0.64$ for this case, the influence of the spurious saddles persists even at this high frequency. On the other hand, the choice $\epsilon = -\delta(1 + 0.001i)$ gives an error of less than

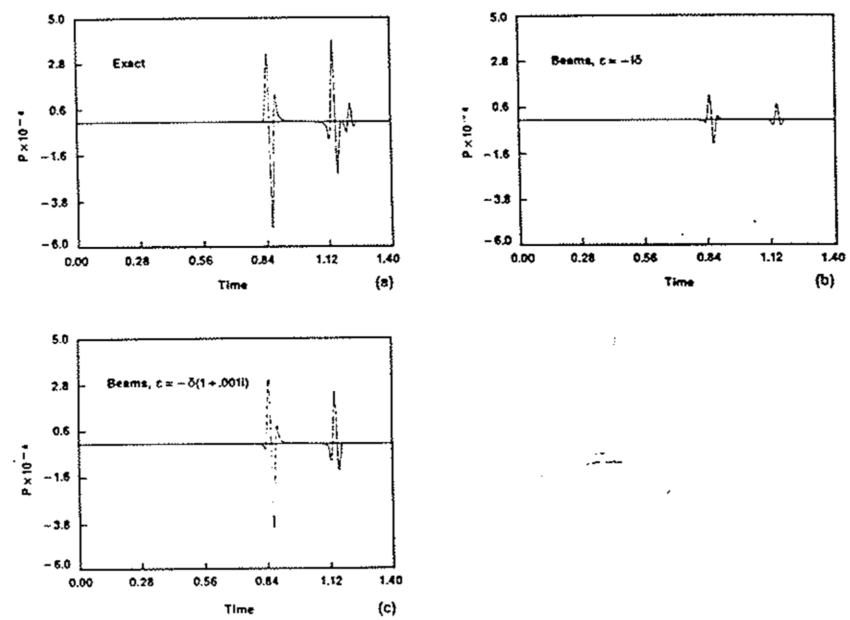

Figure 15. Reflections from a circular cylinder of radius 500 ft, at a depth of 2500 ft for coincident source and receiver. (a) 'Exact' solution obtained by separation of variables; (b) beam solution, $\epsilon = -i\delta$; (c) beam solution is $\epsilon = -\delta_0(1 + 0.001i)$.

2 per cent at 20 Hz, even though the beam width at the interface is 1262 ft, more than twice as large as the cylinder radius.

That the beam width be much smaller than the cylinder radius is implied under some conditions by the 'Fresnel-2 condition', inequality (8.8) of Ben-Menahem & Beydoun (1985). In our notation this inequality becomes $\lambda|A/B| < 2\pi a^2$, and is satisfied for *all* the situations in the preceding paragraph. There $2\pi a^2 = 1\,570\,796$. For $\epsilon = \epsilon_c$, $\lambda|A/B| = 468\,615$ at 20 Hz, and 9372 at 1000 Hz. For $\epsilon = -\delta(1+0.001i)$ and $f = 20$ Hz, $\lambda|A/B| = 60\,001$.

We postpone a discussion of what one can expect as $\epsilon \to -\delta$ until Section 10.

7 The syncline: optimizing ϵ

We here return to the syncline discussed in Section 5, and investigate an alternative choice of the parameter ϵ. We analyse only the case of coincident source and receiver. Then, as shown in Section 5, there are three rays contributing to the field at the receiver, and for the choice of parameters given in Section 5, the beam integral is determined by saddle points at, $\theta_1 = 0$, $\theta_2 = -\theta_3 = 0.048\pi$, as well as any spurious saddles that may accompany a given choice of ϵ. To determine the location and influence of the spurious saddles would require fourth derivatives with respect to θ of the complex phase $\bar{\phi}$, information that could be obtained through higher-order transport equations such as (4.12). The result would then depend upon fourth derivatives of the interface. We will use, instead, a simpler criterion for choosing ϵ, consistent with the prescription for the cylinder, derived in Section 6, that ϵ should be near $-\delta$, in the lower half-plane. From (4.13), we may re-interpret this condition as requiring that the second derivatives of the phase at the true saddles be large. That is, we steepen the steepest descent paths at the true saddle points $\theta_1, \theta_2, \theta_3$. Because of symmetry, we need only consider the trade-off of steepnesses between θ_1 and θ_2.

For $j = 1, 2$ we define the steepness measures

$$Q_j = -c_0 \operatorname{Re} i\bar{\phi}_{\theta\theta}(\theta_j). \tag{7.1}$$

Let $A_1^{(j)}$, $A_2^{(j)}$ be the real ray-tube areas for θ_j, and $\delta_j = A_1^{(j)}/A_2^{(j)}$, as in (4.17). Numerical computation gives $\delta_1 = 1816.2$, $\delta_2 = 2765.7$ for this example. Then from (4.13) Q_j may be written explicitly as a function of ϵ

$$Q_j = -\delta_j \operatorname{Im}\left(\frac{\epsilon}{\epsilon+\delta_j}\right). \tag{7.2}$$

For $\epsilon = \epsilon_1 + i\epsilon_2$ with ϵ_1, ϵ_2 real, $\epsilon_2 < 0$

$$Q_j = \frac{-\delta_j^2\epsilon_2}{[(\epsilon_1+\delta_j)^2+\epsilon_2^2]}. \tag{7.3}$$

Thus $Q_j > 0$.

From (7.3) the curve in the complex ϵ-plane on which $Q_j = q_j$, a constant, is the circle Γ_j with centre at

$$\epsilon^{(j)} = -\delta_j - i\,\frac{\delta_j^2}{2q_j} \tag{7.4}$$

and radius

$$\gamma^{(j)} = \frac{\delta_j^2}{2q_j}. \tag{7.5}$$

That is, the circle Γ_j is in the lower half-plane, and is tangent to the ϵ_1-axis at $\epsilon = -\delta_j$. The radius of the circle shrinks as Q_j is increased. Clearly, then, a pair of values q_1, of Q_1 and q_2 of Q_2 can be attained simultaneously if and only if Γ_1, Γ_2 intersect, the point(s) of intersection being the value(s) of ϵ which produce these values of Q_1, Q_2. That is, q_1, q_2 can be achieved if and only if

$$q_1q_2 < \left|\frac{1}{\delta_1} - \frac{1}{\delta_2}\right|^{-2}. \tag{7.6}$$

Since we wish to make q_1, q_2 as large as possible, we take equality in (7.6)

$$q_1 = \frac{1}{\alpha}\left|\frac{1}{\delta_1} - \frac{1}{\delta_2}\right|^{-1}$$

$$q_2 = \alpha\left|\frac{1}{\delta_1} - \frac{1}{\delta_2}\right|^{-1} \tag{7.7}$$

for some $\alpha > 0$.

Geometrically, equality holds in (7.6) when Γ_1, Γ_2 are tangent. The point of tangency is at

$$\epsilon^* = \frac{-\delta_1\delta_2}{(\delta_1^2/q_1 + \delta_2^2/q_2)}\left(\frac{\delta_1}{q_1} + \frac{\delta_2}{q_2} + i\,\frac{\delta_1\delta_2}{q_1q_2}\right). \tag{7.8}$$

The choice $\alpha = 5$ biases the trade-off of q_1, q_2 toward the double contribution from θ_2, θ_3. Then (7.8) yields for our example, $\epsilon^* = -2687 - 265i$.

Fig. 14 shows how the choice ϵ^* improves the beam solution for the case of coincident source and receiver, for which it was derived. This same value of ϵ^* also gives good results for a wide range of receiver positions, as illustrated in Figs 5(e) and 9(e). Thus the precise optimization of ϵ is not necessary, ϵ need only be in the correct region of the complex plane. The formulas of this section apply in general inhomogeneous media, provided it is only necessary to compromise between two arrivals.

8 Critical angle and head-wave effects

We consider the simple example shown in Fig. 16. A point source is located above a flat interface separating two homogeneous media. The wavespeed of the lower region exceeds

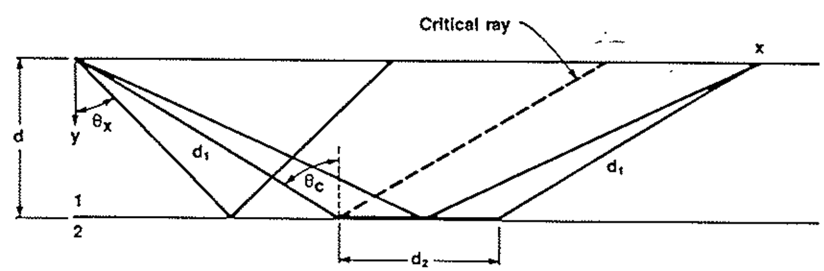

Figure 16. Head waves and reflected rays.

that of the layer, $c_1 < c_2$, so that head-wave effects are expected at receivers where the reflected ray angle θ_x exceeds the critical angle θ_c,

$$\theta_c = \sin^{-1}(c_1/c_2). \tag{8.1}$$

Similar configurations have been considered by Konopaskova & Červený (1984), Nowack & Aki (1985) and by Červený (1983, 1985). We compare our findings to theirs later.

The total field at a receiver $(x, 0), x > 0$ is

$$u^{\text{tot}} = G(\underset{\sim}{x}, \underset{\sim}{x}_0) + u^{\text{ex}}, \tag{8.2}$$

where $\underset{\sim}{x}_0 = (0, 0)$ and G, defined in (5.22), is the 2-D Green function for a point source at $\underset{\sim}{x}_0$. The quantity u^{ex} in (8.2) is the exact scattered field due to the presence of the interface. By the usual methods (Brekhovskikh 1980) we have

$$u^{\text{ex}} = \frac{-i}{4\pi} \int_\Gamma R(\theta) \exp\,[i\lambda \cos(\theta - \theta_x)]\; d\theta \tag{8.3}$$

where

$$\lambda = \omega r/c_1, \tag{8.4a}$$

$$r = (x^2 + 4d^2)^{1/2}, \tag{8.4b}$$

and Γ is the Sommerfeld contour, going from $\theta = -\pi/2 + i\infty$ to $\theta = -\pi/2$, then to $\theta = \pi/2$ and finally to $\theta = \pi/2 - i\infty$. The reflection coefficient $R(\theta)$ is given in (3.11). Let u^{gb} be the beam integral corresponding to the scattered field. It follows readily by using the method of images that

$$u^{\text{gb}} = \frac{-i}{4\pi} \int_{-\pi/2}^{\pi/2} R(\theta)\, [1 + (r/\epsilon) \cos(\theta - \theta_x)]^{-1/2}$$

$$\exp\left[i\lambda \left(\cos(\theta - \theta_x) + \frac{1/2 \sin^2(\theta - \theta_x)}{\cos(\theta - \theta_x) + \epsilon/r} \right) \right] d\theta. \tag{8.5}$$

The integrands of (8.3) and (8.5) are similar in that each has a branch point at $\theta = \theta_c$ and a saddle point at $\theta = \theta_x$. We now consider the asymptotic nature of u^{ex} and u^{gb} for $\lambda \gg 1$. It is well known that the leading order contribution to u^{ex} at receivers with θ_x greater than θ_c contains head-wave effects. The head waves are absent for θ_x less than θ_c and a boundary layer region exists in the critical region, i.e. when $\sqrt{\lambda}|\theta_x - \theta_c| = O(1)$. In order to compare u^{gb} with u^{ex} we now derive uniformly asymptotic approximations to both (8.3) and (8.5) that are valid at all receiver locations.

The generic type of integral in (8.3) and (8.5) is

$$u = \int_\Gamma W(\theta) \exp\,[i\lambda Q(\theta, \theta_x)]\; d\theta, \tag{8.6}$$

where W has a branch point at $\theta = \theta_c$ and Q has a saddle point at $\theta = \theta_x$,

$$Q_\theta(\theta_x, \theta_x) = 0, \qquad Q_{\theta\theta}(\theta_x, \theta_x) \neq 0. \tag{8.7}$$

We can safely disregard the essential singularity at $\theta = \theta_x + \pi - \cos^{-1}(\epsilon/r)$ in (8.5) as its contribution is asymptotically negligible. It is convenient to split $W(\theta)$ as follows,

$$W(\theta) = W_1(\theta) + W_2(\theta)\,(\theta - \theta_c)^{1/2}, \tag{8.8}$$

where both W_1 and W_2 are regular in the neighbourhood of $\theta = \theta_c$. For u^{ex}, for example,

$$W_1 = W_1^{\text{ex}} \equiv \frac{-i}{4\pi} \left(\frac{(\mu_1/\mu_2)^2 \cos^2\theta - \sin^2\theta + \sin^2\theta_c}{(\mu_1/\mu_2)^2 \cos^2\theta + \sin^2\theta - \sin^2\theta_c} \right) \tag{8.9a}$$

$$W_2 = W_2^{\text{ex}} \equiv \frac{-i}{4\pi}\, \frac{-2(\mu_1/\mu_2)\cos\theta}{(\mu_1/\mu_2)^2 \cos^2\theta + \sin^2\theta - \sin^2\theta_c} \left(\frac{\sin^2\theta_c - \sin^2\theta}{\theta - \theta_c} \right)^{1/2}. \tag{8.9b}$$

We thus split u in (8.6) as

$$u = u_1 + u_2, \tag{8.10}$$

where the integrand of the integral u_1 has no branch point at $\theta = \theta_c$. The leading order approximation for u_1 follows simply by the method of stationary phase as

$$u_1 \sim \exp\left(-\frac{i\pi}{4}\right) \left(\frac{2\pi}{\lambda}\right)^{1/2} W_1^{\text{ex}}(\theta_x) \exp(i\lambda) \tag{8.11}$$

for both u^{ex} and u^{gb}. Any differences in the asymptotic forms of u^{ex} and u^{gb} are thus contained only in u_2.

The second integral u_2 is the canonical integral for the coalescence of a saddle point with a branch point singularity. Following Bleistein & Handelsman (1975) we introduce a new variable of integration ξ through the transformation

$$Q(\theta, \theta_x) = -\frac{\xi^2}{2} - \gamma\xi + \beta. \tag{8.12}$$

The parameters γ and β are defined by specifying that $\xi = 0$ is the image of $\theta = \theta_c$ and $\xi = -\gamma$ is the image of $\theta = \theta_x$. Thus,

$$\beta = Q(\theta_c, \theta_x) \tag{8.13a}$$

$$\gamma^2 = 2[Q(\theta_x, \theta_x) - Q(\theta_c, \theta_x)]. \tag{8.13b}$$

We note that for both u^{ex} and u^{gb},

$$\beta = 1 - \gamma^2/2 \tag{8.14}$$

which with (8.12) implies

$$Q(\theta, \theta_x) = 1 - \tfrac{1}{2}(\xi + \gamma)^2. \tag{8.15}$$

Also

$$\gamma = \begin{cases} 2\sin(\alpha/2) & \text{for } u^{\text{ex}} \\ 2\sin(\alpha/2) \left(\dfrac{1 - (r/\epsilon)\sin^2(\alpha/2)}{1 + (r/\epsilon)\cos\alpha} \right)^{1/2} & \text{for } u^{\text{gb}}, \end{cases} \tag{8.16}$$

where

$$\alpha = \theta_x - \theta_c \tag{8.1'}$$

The canonical integral is now

$$u_2 = \exp(i\lambda) \int_{\hat\Gamma} W_2(\theta)\,(\theta - \theta_c)^{1/2} \frac{d\theta}{d\xi} \exp\,[i(\lambda/2)(\xi + \gamma)^2]\; d\xi, \tag{8.1}$$

where $\hat{\Gamma}$ is the image of Γ in the ξ-plane. Next, we write

$$M(\xi) \equiv W_2(\theta)\left(\frac{\theta-\theta_c}{\xi}\right)^{1/2}\frac{d\theta}{d\xi}$$

$$= b_0 + b_1\xi + \xi(\xi+\gamma)N(\xi), \tag{8.19}$$

where

$$b_0 = M(0)$$

$$= W_2(\theta_c)[-\gamma/Q_\theta(\theta_c,\theta_x)]^{3/2} \tag{8.20a}$$

$$b_1 = [M(0) - M(-\gamma)]/\gamma$$

$$= \frac{b_0}{\gamma} - \frac{W_2^{ex}(\theta_x)}{\gamma}(-\alpha/\gamma)^{1/2} \tag{8.20b}$$

The latter result, (8.20b), follows readily from the specific forms of W_2 and Q for both u^{ex} and u^{gb}. The last term in (8.19) vanishes at both critical points. Its asymptotic contribution u_2 can be neglected (see Bleistein & Handelsman 1975) and we obtain,

$$u_2 \sim \frac{\exp[i\lambda(1-\gamma^2/2)]}{\lambda^{3/4}}\left(b_0 E(\sqrt{\lambda}\gamma) + \frac{ib_1}{\sqrt{\lambda}}E'(\sqrt{\lambda}\gamma)\right). \tag{8.21}$$

The function E is

$$E(z) = \int_{-\infty+i0}^{\infty-i0} s^{1/2}\exp[-i(s^2/2+zs)]\,ds \tag{8.22}$$

which is related to the parabolic cylinder function $D_{1/2}$ (Gradshteyn & Ryzhik 1980, equation 9.241.1) as follows,

$$E(z) = \sqrt{2\pi}\exp(i\pi/8)\exp(iz^2/4)D_{1/2}[\exp(-i\pi/4)z]. \tag{8.23}$$

The uniform asymptotic approximation of u of (8.6) follows from (8.10), (8.11) and (8.21). This solution contains the usual specularly reflected field for pre-critical incidence, $\theta_x < \theta_c$, plus head-wave effects for post-critical incidence. The transition between the two regimes occurs when $|\sqrt{\lambda}\gamma| = 0(1)$. We first consider pre-critical incidence, $|\sqrt{\lambda}\gamma| \gg 1$ and $\alpha = \theta_x - \theta_c < 0$. Then the appropriate asymptotic expansion of $D_{1/2}$ (Gradshteyn & Ryzhik 1980, equation 9.246.1) gives

$$u_2 \sim \exp(-i\pi/4)\frac{2\pi^{1/2}}{\lambda}W_x^{ex}(\theta_x)\sqrt{\theta_x-\theta_c}\exp(i\lambda) \tag{8.24}$$

for both u^{ex} and u^{gb}. Combining (8.11) and (8.24), we get, for pre-critical incidence,

$$\left.\begin{matrix}u^{ex}\\u^{gb}\end{matrix}\right\} = u^{ref}[1+0(\lambda^{-1})], \tag{8.25}$$

where

$$u^{ref} \equiv \frac{\exp(-3\pi i/4)}{\sqrt{8\pi\lambda}}R(\theta_x)\exp(i\lambda). \tag{8.26}$$

The case of post-critical incidence, $\alpha > 0$, requires a different asymptotic expansion of $D_{1/2}$ (Gradshteyn & Rzyhik 1980, equation 9.246.3). This time we get different results for u_2 for the beams and the exact solutions. The combined solutions $u_1 + u_2$ now depend on the parameter γ of (8.16). We have,

$$u = u^{ref}[1+0(\lambda^{-1})] + u^{crit}[1+0(\lambda^{-1})], \tag{8.27}$$

where

$$u^{crit} = \frac{-\sqrt{\pi}W_2(\theta_c)\exp[i\lambda(1-\gamma^2/2)]}{[-\lambda Q_\theta(\theta_c,\theta_x)]^{3/2}}. \tag{8.28}$$

The difference between u^{ex} and u^{gb} comes from the term u^{crit}. In both cases we have

$$\lambda(1-\gamma^2/2) = \lambda Q(\theta_c,\theta_x). \tag{8.29}$$

In the exact solution u^{crit} is the head-wave (or lateral wave) contribution. The phase in this case is

$$\lambda Q(\theta_c,\theta_x) = \lambda\cos\alpha$$

$$= \omega\left(\frac{2d_1}{c_1} + \frac{d_2}{c_2}\right), \tag{8.30}$$

where d_1 and d_2 are defined in Fig. 16. We note also that in the exact solution

$$-\lambda Q_\theta(\theta_c,\theta_x) = \lambda\sin\alpha$$

$$= \frac{\omega d_2}{c_1}\cos\theta_c \tag{8.31}$$

and hence the head-wave amplitude decays as $(d_2)^{-3/2}$.

However, u^{crit} does not give the head waves correctly for u^{gb}. First, the amplitude is incorrect since both $W_2(\theta_c)$ and $Q_\theta(\theta_c,\theta_x)$ are not the same as for u^{ex}. The phase error is more grievous, since now we have

$$\lambda Q(\theta_c,\theta_x) = \omega\left(\frac{2d_1}{c_1} + \frac{d_2}{c_2}\right) + \frac{\omega}{2c_1}\,\frac{(d_2\cos\theta_c)^2}{2d_1 + d_2\sin\theta_c + \epsilon}. \tag{8.32}$$

For finite $|\epsilon|$ with $\epsilon_2 < 0$, the phase λQ in (8.32) has a positive imaginary part proportional to ω. Thus, the head-wave contribution in the beam solution will be exponentially small. For a fixed ϵ, the imaginary part of the phase error increases monotonically with d_2 or $\theta_x - \theta_c$ from zero at $d_2 = 0$ to $(-\epsilon_2\omega/2c_1)\cot^2\theta_c$ as $d_2 \to \infty$. Only in the limiting case of $|\epsilon|/r \gg 1$ does u^{gb} have the correct head-wave contribution. This limit is analogous to a plane wave decomposition of the source, so it is not surprising that the correct solution is obtained. In fact, the uniformly asymptotic result (8.21) for u_2^{gb} reduces to u_2^{ex} when $|\epsilon|/r \gg 1$, as one would expect. However, this asymptotic agreement is contingent upon the condition that the end point contributions to the beam integral of $\theta = \pm\pi/2$ are negligible. This is *not* true in the limit $|\epsilon|/r \to \infty$, in which case the beam integral equals the exact solution minus the evanescent-wave contribution to u_{ex}. We have verified this circumstance numerically.

Finally, we note that near critical incidence, i.e. in the critical region $|\alpha| = 0(\lambda^{-1/2})$, the beams and exact solutions agree to first order in α. In summary, the beams give good results in the regular ray region and in the critical region but in general fail to give the correct head-wave effects in the post-critical region except in the limit of $|\epsilon|/r \gg 1$.

COMPARISON WITH NUMERICAL RESULTS

In order to verify the above findings we have computed the signal at various receiver locations for the same problems as in Section 5, minus the syncline. Thus, $d = 2000$, $c_1 = 6000$ and $c_2 = 7000$. Three signals were calculated at each receiver: the exact solution (8.3), the Gaussian beam solution (8.5) and the 'naive' ray theory solution (8.26). The critical receiver distance is approximately 6650. The results of Fig. 17 are for $x = 3000$ from which we see that all three methods are in good agreement for pre-critical incidence. However, near critical incidence, it can be seen from Fig. 18 that naive ray theory is in serious error while the beams do significantly better, as we predicted. The values of ϵ chosen in Figs 8.2 and 8.3 are the Červený *et al.* (1982) optimal values of (4.16), in this case $\epsilon = -i\lambda$, where λ is defined in (8.4a). Fig. 19 shows the three solutions for a receiver well into the head-wave region. The distinct head wave and reflected signals can be seen in Fig. 19(a). However, the head wave is absent from the Gaussian beam result, because we have used the Červený optimal ϵ. By increasing $|\epsilon|$, as in Fig. 20, we obtain the head-wave contribution.

The above findings also corroborate and explain previously published numerical results of Červený (1983), Konopaskova & Červený (1984, I and II), and Nowack & Aki (1985), among others. Each of these papers considers a configuration similar to ours. Let us discuss the papers of Konopaskova & Červený (1984, I and II) first, since they investigate in depth the sensitivity of the Gaussian beam method.

The relevant parameters in Konopaskova & Červený (1984, I and II) are $d = 30$ km, $\theta_c = \sin^{-1}(4/5)$, and therefore the critical distance is $x_c = 80$ km. The typical value of r in

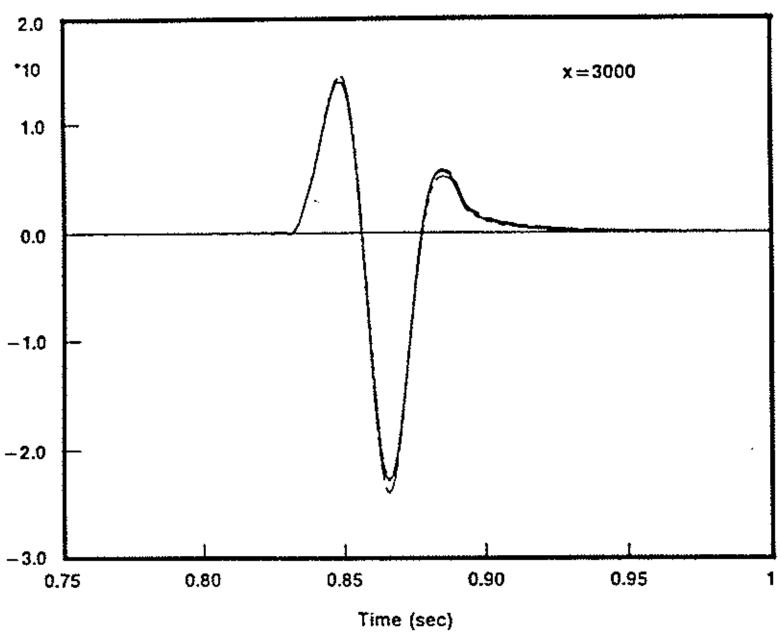

Figure 17. Pre-critical incidence, $x = 3000$. The critical distance is 6650. There are three distinct curves, corresponding to exact ——, beam – –, and rays – · · · –.

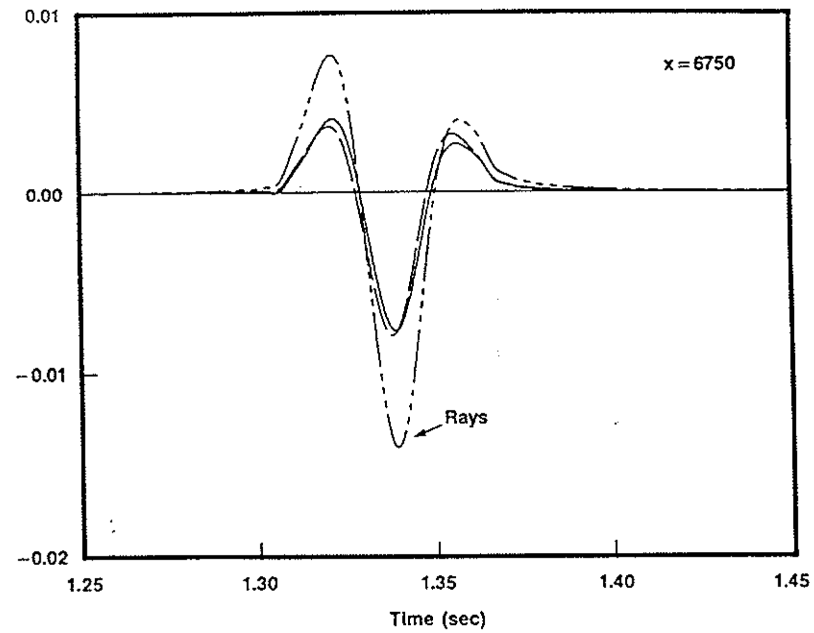

Figure 18. Near critical incidence, $x = 6750$. The three curves are distinguished as in Fig. 17.

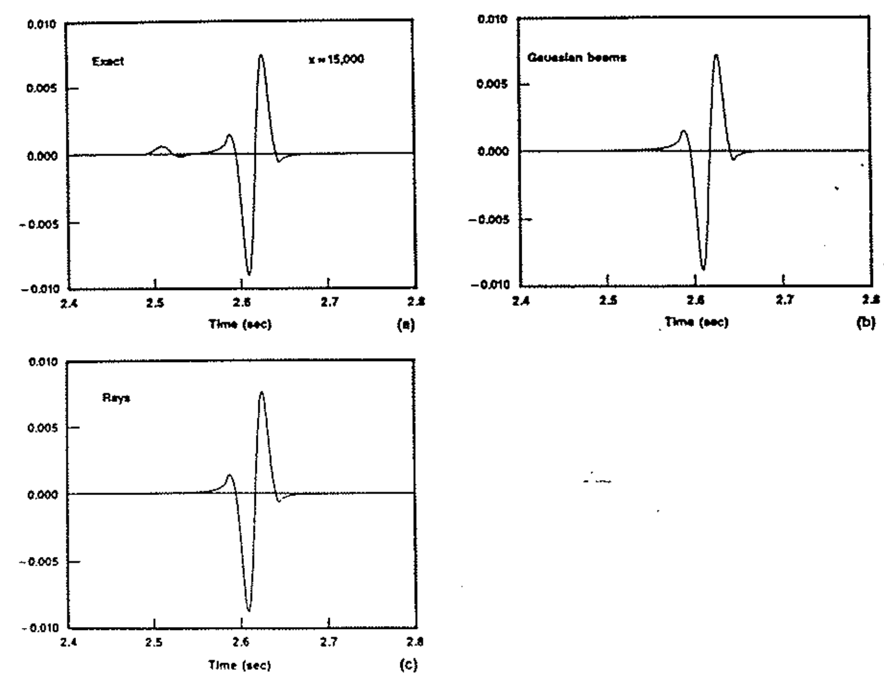

Figure 19. Receiver well inside the head-wave zone, $x = 15000$. The ϵ used for the beam solution is the optimal value of equation (4.16).

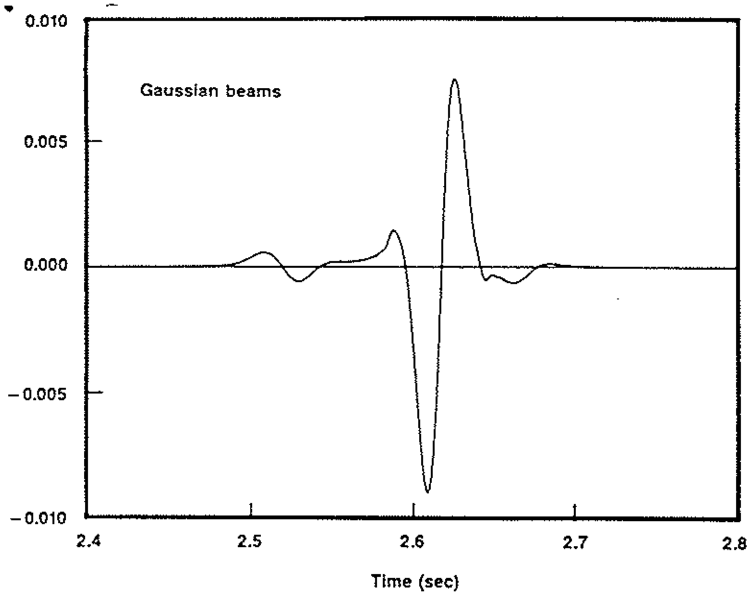

Figure 20. A Gaussian beam solution at $x = 15\,000$ with ϵ equal to 25 times the optimal value of equation (4.16).

the critical region is thus 100 km or more. Also $c_1 = 6.4\ \mathrm{km\ s^{-1}}$, and the centre frequency is 6.4 Hz, so that $\lambda = 200\pi$, which is certainly much larger than unity. The parameter ϵ is $\epsilon = -i\pi L_0^2/c_1$ in KMS units, where L_0 defines the beam half-width at the source. The 'optimal' value of ϵ as defined by Červený *et al.* (1982), is $i\epsilon = r$, or $L_0 \approx 14$ km. Konopaskova & Červený (1984, I) take L_0 so that $|\epsilon/r| = 25$, or $L_0 \approx 70$ km, and find the beams to be in very good agreement with the exact solution. In fact, in II, they surmise from numerical results that the beams are exact in the limit $|\epsilon|/r \to \infty$, in accordance with our analysis. In II they also experiment with small values of L_0, and observe that the beams are qualitatively correct in the critical region but can have slightly erroneous amplitudes, on the order of 2–10 per cent. The latter effect is probably due to the finite nature of $\alpha = \theta_x - \theta_c$. All their results show the beam integral to be in excellent agreement with the exact solution in the pre-critical or regular region.

Konopaskova & Červený (1984, I and II) considered only the total amplitudes u^{ex} and u^{gb}. The error in the head waves in the post-critical region was therefore not apparent because the reflected arrivals dominate there. Červený (1983) investigated the same configuration and showed synthetic seismograms for receivers located past x_c. He chose L_0 to be close to the optimal value, so that we would expect the beams to give 'head-wave' contributions of exponentially small amplitude. The fact that his plots showed no signs of head waves was a matter of concern to Červený, but is totally in agreement with our findings. In fact, the absence of head waves in his computations is evidence of the accuracy of his numerical integration. Nowack & Aki (1985) presented results similar to Červený's for values of L_0 much greater than the optimum. They observed head waves for $|\epsilon|/r \gtrsim 10$ but none for smaller L_0, again in agreement with our results. Finally, we note that a recent review (Červený 1985) discusses the same numerical example as Konopaskova & Červený.

In the review, Červený notes that 'head waves are obtained only if the width of Gaussian beams is rather large'.

9 Diffraction by a half-plane

9.1 THE BEAM INTEGRAL: THE FREQUENCY AND THE TIME-DEPENDENT VERSIONS

Suppose that in a uniform medium a plane wave of the form

$$u_{\mathrm{inc}} = \exp(ikx), \qquad k = \omega/c \tag{9.1}$$

impinges on a semi-infinite straight screen with edge at the origin and extending into the fourth quadrant of the xy plane. The Gaussian beam superposition method prescribes that we express u_{inc} as a superposition of Gaussian beams:

$$\exp(-ikx) = \int_{-\infty}^{\infty} \left(\frac{-ik}{2\pi(-x+\epsilon)}\right)^{1/2} \exp\left[ik\left(-x + \frac{(y-\eta)^2}{2(-x+\epsilon)}\right)\right] d\eta. \tag{9.2}$$

The integrand for each η represents a single Gaussian beam with axis along the line $y = \eta$ and travelling in the negative x direction. The diffracting screen intercepts all those beams which lie in the half plane $y < 0$, namely those for which $\eta < 0$, and the method prescribes that such beams contribute nothing to the field in $x < 0$. Thus the field in $x < 0$ is approximated by

$$u = \left(\frac{-ik}{2\pi(-x+\epsilon)}\right)^{1/2} \int_{0}^{\infty} \exp\left[ik\left(-x + \frac{(y-\eta)^2}{2(-x+\epsilon)}\right)\right] d\eta. \tag{9.3}$$

By a simple change of variable of integration (9.3) can be written as

$$u = \left(\frac{-ik}{2\pi(-x+\epsilon)}\right)^{1/2} \int_{-\infty}^{y} \exp\left[ik\left(-x + \frac{1}{2}\frac{y'^2}{(-x+\epsilon)}\right)\right] dy'. \tag{9.4}$$

At this point we will leave the frequency domain and Fourier transform back to the time domain. We make use of the fact that when $\mathrm{Im}\,\tau > 0$ and $\omega > 0$

$$\int_{-\infty}^{\infty} \mathrm{Re}\,[a(t-\tau)^{-3/2}]\,\exp(i\omega t)\,dt = a(-3/2)!\,(-i\omega)^{1/2}\exp(i\omega\tau). \tag{9.5}$$

Thus we see from (9.5) that the time-domain inversions of (9.2) and (9.4) are

$$\delta\left(t + \frac{x}{c}\right) = \int_{-\infty}^{\infty} \frac{1}{(-3/2)!\,\sqrt{2\pi c}}\,\mathrm{Re}\left(\frac{1}{(-x+\epsilon)^{1/2}}\,\frac{1}{[\![t + x/c - (y-\eta)^2/[2(-x+\epsilon)]]\!]^{3/2}}\right) d\eta \tag{9.6}$$

$$u = \frac{1}{(-3/2)!\,\sqrt{2\pi c}}\,\mathrm{Re}\left(\int_{-\infty}^{y} \frac{1}{(-x+\epsilon)^{1/2}}\,\frac{1}{[\![t + x/c - y'^2/[2c(-x+\epsilon)]]\!]^{3/2}}\,dy\right). \tag{9.7}$$

Conveniently the integral in (9.7) is elementary:

$$u = \frac{-1}{2\pi}\,\mathrm{Re}\left[\frac{1}{t + x/c - 0i}\left(\frac{y/\sqrt{c}}{[2(t+x/c)(-x+\epsilon)(-y^2/c)]^{1/2}} + i\right)\right] \tag{9.8}$$

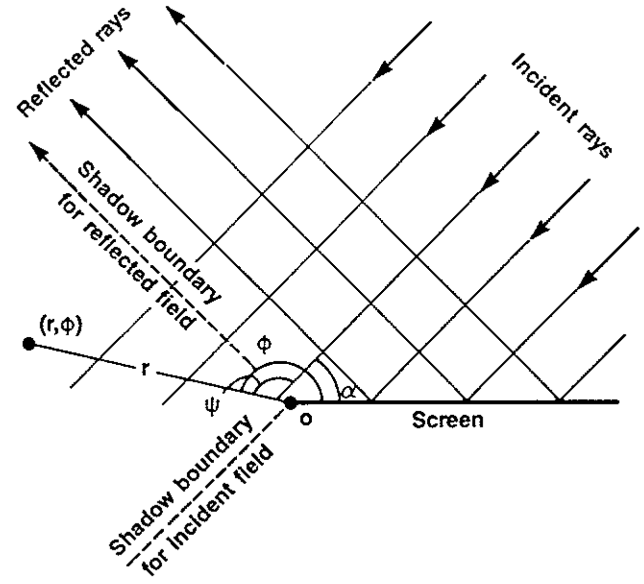

Figure 21. A schematized diffracting screen, incident field and reflected field. The polar angles α, ϕ, ψ described in the text are shown.

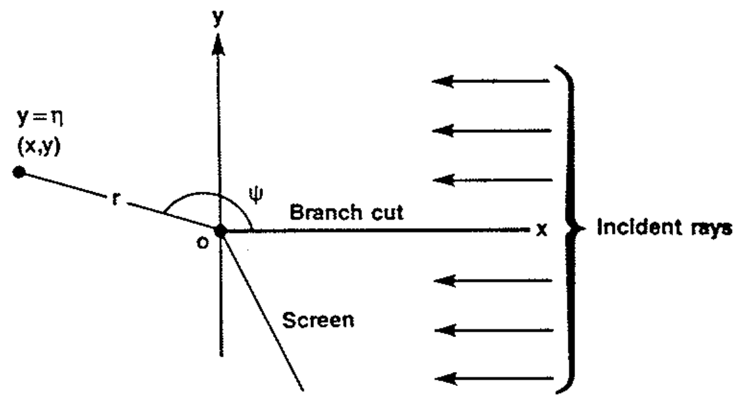

Figure 22. The coordinate system x, y, r, ψ used in (9.8) and (9.13). The term $U(r, x)$ in Sommerfeld's solution and u of Subsection 9.1 are double valued in this plane unless a branch cut is inserted along the x-axis, for instance.

It is worth remarking that often the range of integration is truncated in the beam integral even when there are no screens or other diffracting obstacles. In that case we would expect to see associated artefacts resembling the diffraction-like events in the beam integrals considered here and displayed in Figs 23(b), (c)–29(b), (c). In other sections of this paper we have avoided such spurious end effects, but their general character can be inferred from the description in this section.

9.2 THE SOMMERFELD SOLUTION AND ITS TIME-DEPENDENT ANALOGUE

Sommerfeld (1954) (after Sommerfeld 1896) gives the exact solution for the field when a plane wave impinges on a straight screen at angle α (see Figs 21 and 22). His expression is

$$u = U(r, \phi - \alpha) - U(r, \phi + \alpha), \tag{9.9}$$

where α is the angle between the screen and the direction from which the incident field is travelling, r, ϕ are polar coordinates with origin at the edge of the screen and ϕ is measured from the screen, and

$$U(r, \psi) = \frac{\exp\,[-i(\pi/4)]}{\sqrt{\pi}} \exp(ikx) \int_{-\infty}^{\rho} \exp(is^2)\, ds \tag{9.10}$$

$$\rho = \sqrt{2kr} \cos\frac{\psi}{2} \tag{9.11}$$

It turns out that U, like u of (9.4), has a time-dependent analogue which is an elementary integral. First extract $k^{1/2}$ from the variable of integration to get

$$U(r, \psi) = \frac{(-ik)^{1/2}}{\sqrt{\pi}} \exp(-ikx) \int_{-\infty}^{\sqrt{2r}\cos(\psi/2)} \exp(ik\sigma^2)\, d\sigma \tag{9.12}$$

Then again by (9.5) we recognize this as the Fourier transform of

$$\begin{aligned} U(r, \psi) &= \frac{1}{(-3/2)!} \frac{1}{\sqrt{\pi c}} \operatorname{Re} \int_{-\infty}^{\sqrt{2r}\cos(\psi/2)} \frac{d\sigma}{(\tau + x/c - \sigma^2/c - 0i)^{3/2}} \\ &= \frac{1}{-2\pi} \operatorname{Re} \left(\frac{\sigma/\sqrt{c}}{(t + x/c - 0i)(t + x/c - \sigma^2/c - 0i)^{1/2}} \right)_{\sigma = -\infty}^{\sigma = \sqrt{2r}\cos(\psi/2)} \\ &= \frac{-1}{2\pi} \operatorname{Re} \left[\frac{1}{(t + x/c - 0i)} \left(\frac{(\sqrt{2r/c})\cos(\psi/2)}{(t - r/c - 0i)^{1/2}} + i \right) \right]. \end{aligned} \tag{9.13}$$

Thus,

$$u(r, \psi) = \delta\left(t + \frac{x}{c}\right) H\left(\cos\frac{\psi}{2}\right) - \frac{(\sqrt{2r/c})\cos(\psi/2)}{\pi(t + x/c)\sqrt{t - r/c}}. \tag{9.14}$$

In this subsection we have identified ψ with the polar angle measured from the direction from which the incident wave is travelling and then written

$$x = r\cos\psi. \tag{9.15}$$

This conforms with the convention in subsection 9.1.

9.3 COMPARISON OF (9.8) and (9.13)

It is interesting that by a suitable choice of ϵ (9.8) can be made to agree with (9.13). Thus if we choose ϵ so that the phases (arrival times) of the edge-diffracted arrival agree:

$$-x + \frac{y^2}{2(-x + \epsilon)} = r, \tag{9.16}$$

where the left and right members are the values of ct which make the argument of the reciprocal square roots in (9.8), (9.13) vanish. Then

$$-x+\epsilon=\frac{y^2}{2(r+x)}=(r-x)/2 \tag{9.17}$$

$$\epsilon=(r+x)/2. \tag{9.18}$$

On making use of (9.18) and the fact that

$$\sqrt{2r}\cos\frac{\psi}{2}=\sqrt{r+x}\,\operatorname{sgn} y,\ \frac{\pi}{2}<\psi<\frac{3\pi}{2} \tag{9.19}$$

we see that not only do the arrival times agree but the whole expressions (9.8) and (9.13) for u and U agree. But the value of ϵ in (9.18) is real and so does not correspond to a true Gaussian beam but to a limiting degenerate form with zero width at the waist and infinite width elsewhere. Moreover ϵ depends upon the field point and so even when ϵ is chosen according to (9.18) the field is only accurate on the parabola of field points having the same value of $r+x$. However, as we would expect, the truncated incident wave

$$\delta\left(t+\frac{x}{c}\right)H(y) \tag{9.20}$$

is contained in (9.8) and agrees with (9.14). The remaining term represented by the reciprocal square roots in (9.16) and (9.14) differ when ϵ differs from $(r+x)/2$. Because of the factor $(t+x/c)^{-1}$ this diffracted field is largest near the shadow boundary which coincides with the negative x-axis. But here $r+x=0$ and so by choosing $\epsilon=0$ or near 0 (see 9.18) the diffracted field can be made fairly accurate near the shadow boundary, where it is most significant. This choice of ϵ corresponds to choosing the waists of the individual beams to lie on the y-axis and making the beams narrow at the waists.

Actually we have not concerned ourselves with the contribution from the second term $U(r,\phi+\alpha)$ in (9.9). This term represents the reflected field and its diffracted arrival which is most significant near the shadow boundary for the reflected field. Its contribution in $x<0$ will be small and will depend upon α. By contrast the beam superposition integral nowhere makes use of the direction of the screen, nor the x coordinate of its edge, nor whether it is soft or hard. Indeed, if the screen were replaced by a smooth diffractor which intercepted the same beam axes ($\eta<0$) the same final field (9.8) would have been calculated. Since the exact solutions for these different diffractors yield different fields, the beam integral cannot be correct for all of them and, when it is correct, this fact must be regarded as a coincidence. This remark applies to diffraction effects as opposed to phenomena involving specular reflection or refraction at smooth surfaces and propagation in smooth media as at caustics where the beam integral yields reasonably accurate results.

9.4 NUMERICAL ILLUSTRATIONS

To illustrate these results we have made computations using (9.8) and (9.13). We calculate the field at points on the unit circle $r=1$ at various angles between 120° and 240° from the positive x direction. In Figs 23(a), 24(a), 29(a) we display the exact solution (9.13) with $t-0i$ replaced by $t-i\tau$, where τ is non-zero and the delta function representing the incident field is smoothed and more easily represented graphically. Notice in particular the pulse shape and arrival time of the edge diffracted pulse. It is a reciprocal square root pulse

whose singularity arrives precisely at $t=r=1$. In this graphical representation the width of its (positive or negative) peak indicates its amplitude. Notice also for $120°<x<180°$ the incident δ-function pulse is present, arriving at $t=-x=-r\cos\psi$. For $\psi=180°$ the time function consists of precisely one half of the incident field and for $180°<\psi<240°$ there is no arrival corresponding to the incident wave.

The next suite of graphs, labelled (b) in Figs 23–29, shows the corresponding beam integral (9.8) evaluated for $\epsilon=0$. As we intimated in Subsection 9.3, this agrees well with the exact solution near $\psi=180°$. But as ψ deviates further from 180° the time of arrival of the diffracted pulse is delayed more and more relative to the correct arrival time $t=1$. In fact this pulse arrives at $t=-r(\cos\psi+\sec\psi)/2$, which yields $t=1.25$ for $\psi=120°$ and $\psi=240°$. The pulse shape and amplitude are nearly correct as is the representation of the incident wave.

In the next suite of graphs, those labelled (c) in Figs 23–29, ϵ is taken pure imaginary $\epsilon=ix$ (recall $x<0$). In this way the waists of the beams are on the y-axis ($x=0$) and their widths at the field point (x,y) are as narrow as possible, given the waists are on $x=0$. This choice is the optimal ϵ of Červený *et al.* Our graphical output shows that the incident wave is still represented adequately but that the diffracted pulse is grossly smoothed and arrives slightly early.

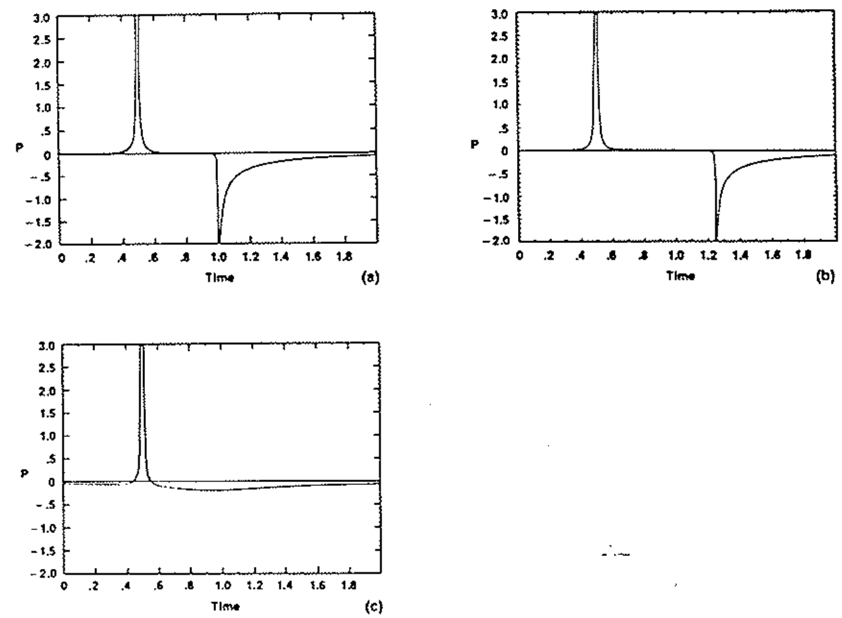

Figure 23. For comparison, the seismograms produced when an impulsive plane wave impinges on a diffracting halfplane. For ease of plotting the incident impulse is slightly smoothed. Here the receiver position is $r=1$, $\psi=120°$ (see text). The exact solution is plotted in (a); notice the direct wave arriving at $t=r\cos\psi=0.5$ and the edge diffraction arriving at $t=r=1$. The beam integral is plotted in (b) for $\epsilon=0$. Notice that the edge-diffracted pulse is late, arriving at $t=-1/2r(\cos\psi+\sec\psi)=1.25$. The beam integral is plotted in (c) for $\epsilon=-i\tau$, optimal from (4.16). The direct arrival is still quite accurate but the edge diffraction is grossly smoothed.

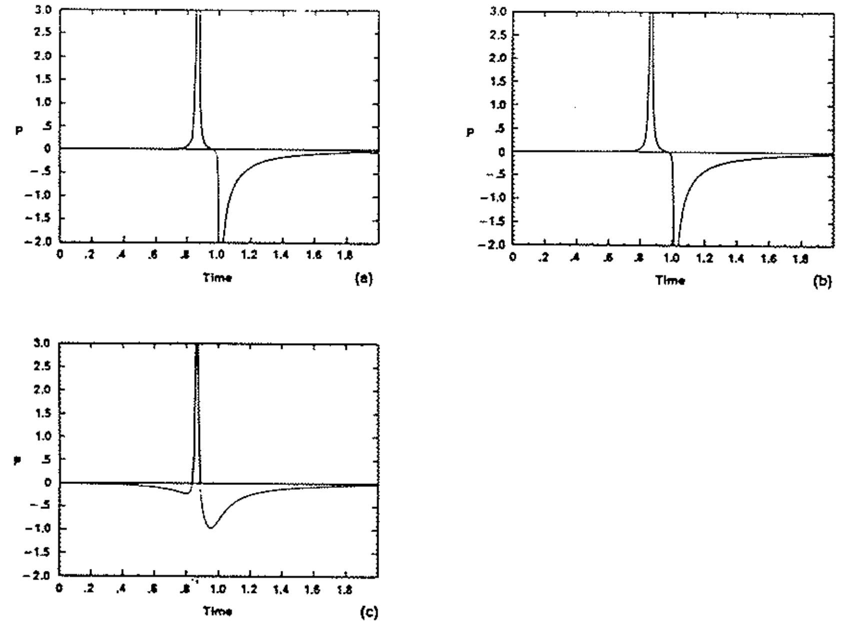

Figure 24. As Fig. 23 except that the receiver position is $r = 1$, $\psi = 150°$. Here the diffracted arrival in Fig. 23(b) is only slightly late, arriving at $t = -\frac{1}{2}r\ (\cos\psi + \sec\psi) = 1.0104$. In (c) the diffracted arrival, while still grossly smoothed, is more prominent.

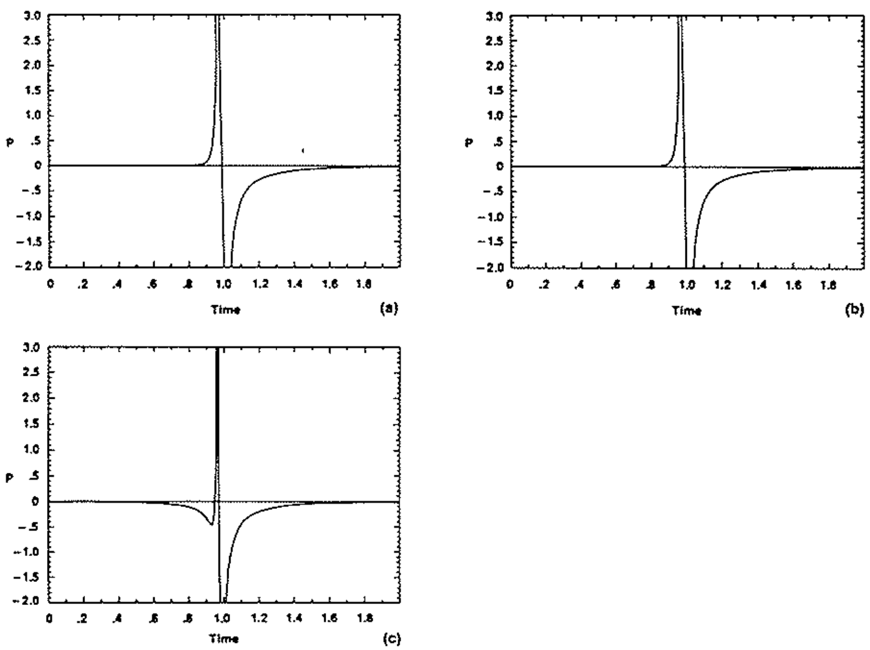

Figure 25. As Fig. 23 except that $\psi = 165°$. This time ψ is near enough to 180° that (b) is indistinguishable from (a). The diffracted arrival in (c) is sharper but gives a negative lobe to the signal before $t = 1$.

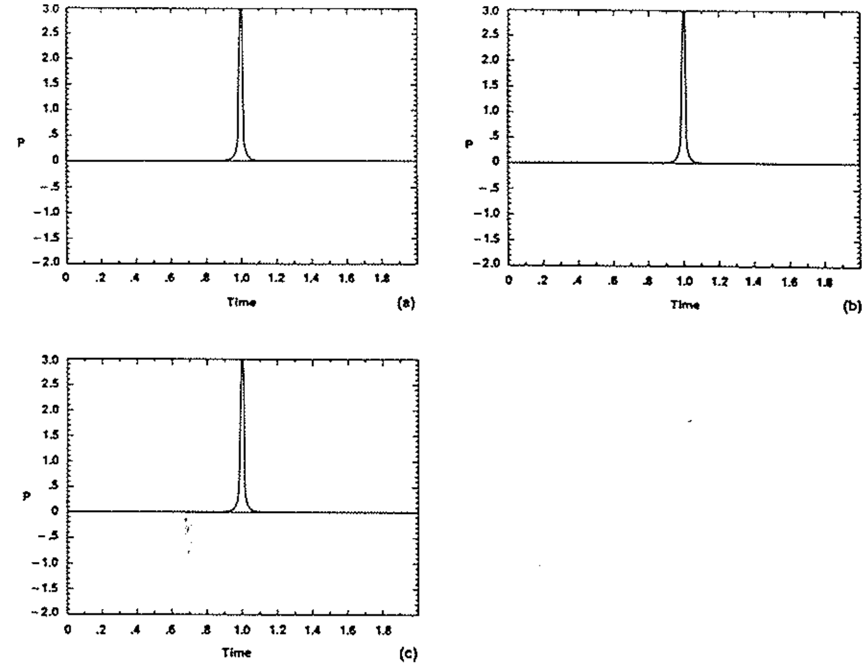

Figure 26. As Fig. 23 except that $\psi = 180°$. Here (a), (b), (c) are indistinguishable.

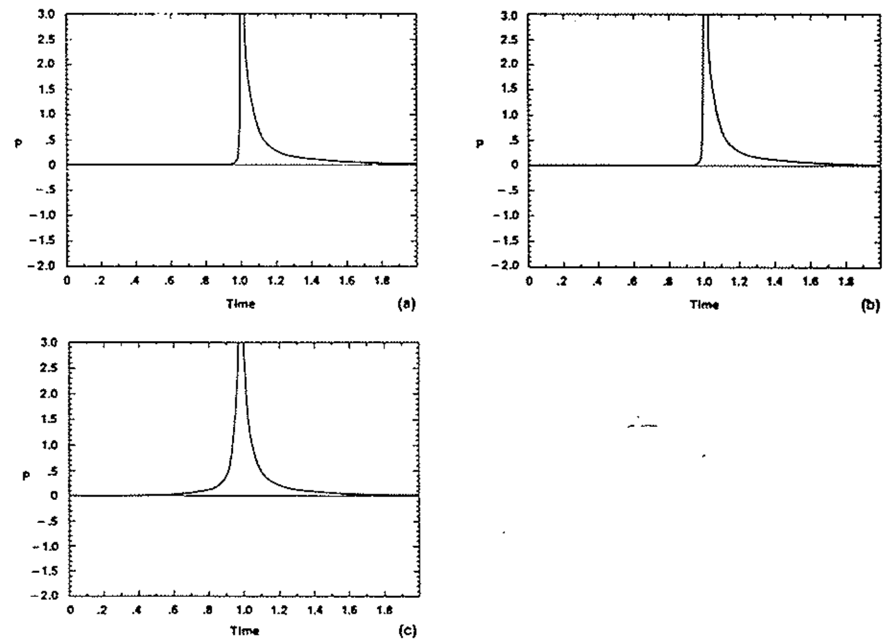

Figure 27. As Fig. 23 except that $\psi = 195°$ which is in the shadow for the incident field which no longer appears. The diffracted field is the same as in Fig. 25 for (a), (b), and (c) but of opposite sign.

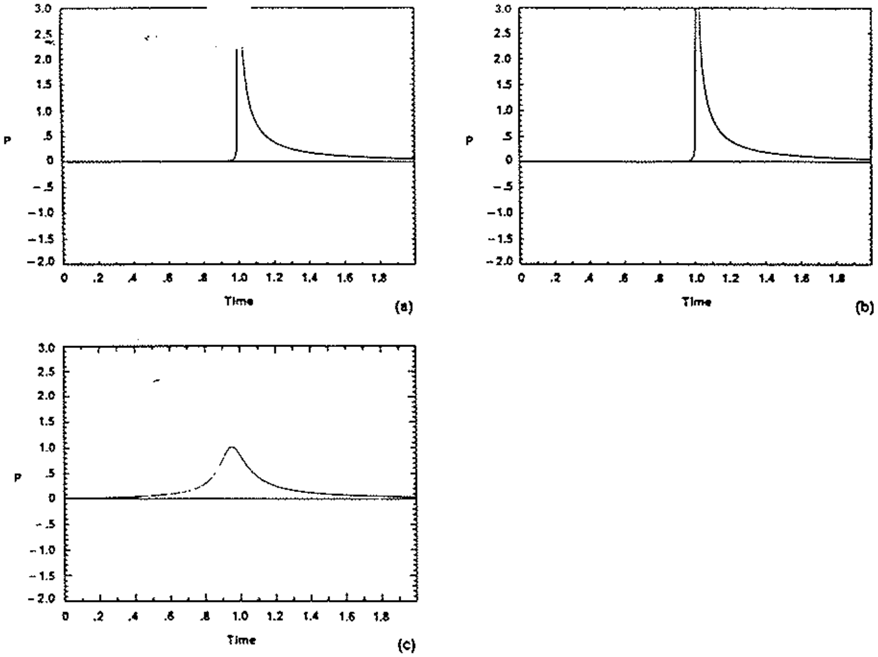

Figure 28. Here $\psi = 210°$. The incident pulse is not present. The diffracted arrival is the same as in Fig. 24 but of opposite sign.

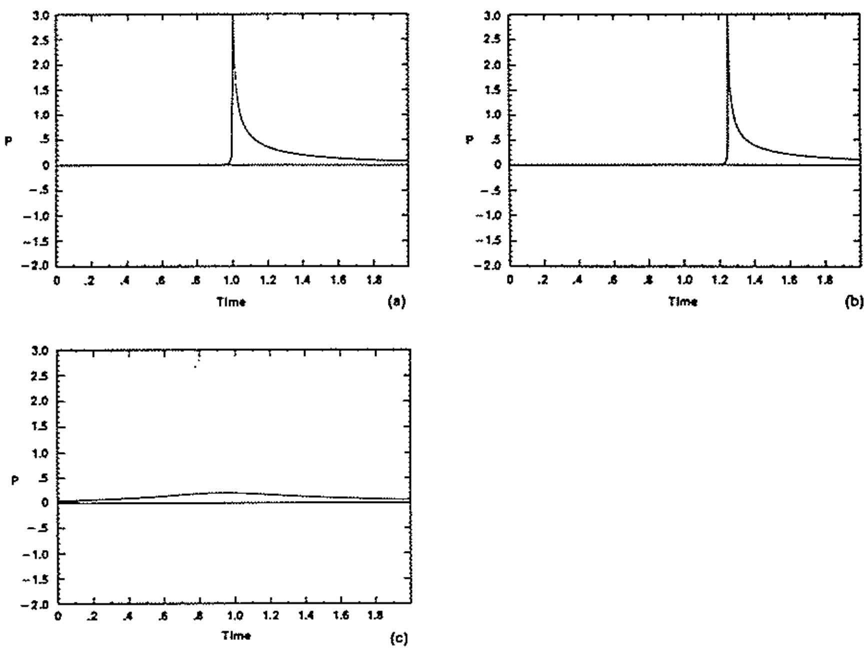

Figure 29. Same as Fig. 28 except that $\psi = 240°$.

10 A singular choice of ϵ

In certain circumstances, the Gaussian beam phase of (4.8) considered as a function of θ can possess a pole in the vicinity of a saddle point. This happens when ϵ is chosen such that A in (4.8) is small for θ near θ_j, where θ_j is the angle of a real ray that reaches the receiver, i.e. $\bar{n}(\theta_j; x_R) = 0$. In this section we consider the canonical integral involved and discuss the effect it has on the calculated field at the receiver.

The usual expansion of the phase near $\theta = \theta_j$ is

$$\bar{\phi}(\theta; x_R) = \tau^{(j)} + 1/2\ \frac{\partial^2 \bar{\phi}}{\partial \theta^2}(\theta_j; x_R)\,(\theta - \theta_j)^2 \tag{10.1}$$

where, from (4.13)

$$\frac{\partial^2}{\partial \theta^2}\bar{\phi}(\theta_j; x_R) = \frac{-\epsilon\delta_j}{(\epsilon + \delta_j)\,c_0} \tag{10.2}$$

and

$$\delta_j = \frac{A_1(\tau^{(j)}, \theta_j)}{A_2(\tau^{(j)}, \theta_j)}. \tag{10.3}$$

Suppose, however that ϵ is chosen as follows,

$$\epsilon = -\delta_j(1 + i\beta), \tag{10.4}$$

where β is real and $|\beta| < 1$, $\beta\delta_j > 0$. Then the quantity A in (4.8) will be zero for some complex value of θ, say θ_p, near θ_j. The expansion (10.1) is now valid only for $\theta - \theta_j = O(\theta_p - \theta_j)$. In order to accommodate this new singularity we must consider the generic form of the phase which contains a pole near a saddle point. To this end we assume that the phase in the neighbourhood of θ_j and θ_p can be written

$$\bar{\phi}(\theta; x_R) = \tau^{(j)} + 1/2\ \frac{\partial^2 \bar{\phi}}{\partial \theta^2}(\theta_j; x_R)\ \frac{\xi_p \xi^2}{\xi_p - \xi}. \tag{10.5}$$

The transformation variable $\xi = \xi(\theta)$ is assumed to have an inverse $\theta = \theta(\xi)$, and, also, to satisfy (i) $\xi(\theta_j) = 0$, (ii) $\xi(\theta_p) = \xi_p$, (iii) $d\xi(\theta_j)/d\theta = 1$ and (iv) $d\xi(\theta_p)/d\theta = 1$. Let the residue of $\bar{\phi}(\theta; x_r)$ at θ_p be R_p, then by (ii) and (iv),

$$\xi_p = \left(-2R_p \Big/ \frac{\partial^2 \bar{\phi}(\theta_j; x_R)}{\partial \theta^2}\right)^{1/3} \tag{10.6}$$

The other two conditions and (10.5) implicitly define the function $\xi(\theta)$.

The pole θ_p occurs when $\epsilon + \delta = 0$, where $\delta = \delta[\tau(\theta; x_R), \theta]$ is defined in (4.17). Near $\theta = \theta_j$, assume that δ can be expanded

$$\delta = \delta_j + \delta_j'(\theta - \theta_j) + O[(\theta - \theta_j)^2], \tag{10.7}$$

where δ_j' is non-zero, which is typically the case. It can happen that $\delta_j' = 0$, for example when the receiver is at $x = y = 0$ in the example of Section 5. This, however, is an exceptional circumstance requiring a different ansatz than (10.5) and will not be considered. With ϵ from (10.4) it follows from (10.7) that

$$\theta_p - \theta_j \sim i\beta_j\delta/\delta_j'. \tag{10.8}$$

The error in (10.8) is of order $\beta^2\delta_j^2/(\delta_j')^3$ which is assumed small compared with (10.8). Using (10.8), it follows from (4.8), (10.2) and (10.6) that

$$\frac{\partial^2\bar{\phi}}{\partial\theta^2}(\theta_j;x_R)\sim\frac{i\delta_j}{c_0\beta} \tag{10.9a}$$

$$R_p\sim-\frac{\beta^2\delta_j^4}{2c_0(\delta_j')^3} \tag{10.9b}$$

$$\xi_p\sim\theta_p. \tag{10.9c}$$

The integral for the field at x_R is given in (4.6). The relevant contribution to this integral from the saddle point θ_j and nearby pole follows from (4.14), (4.15) and (10.5) as

$$\bar{u}^{(j)}(x_R)\sim-(-i)^{K_I}\frac{\exp(i\pi/4)}{\sqrt{8\pi\omega/c^{(j)}}}\frac{\exp(i\omega\tau^{(j)})}{\sqrt{|A^{(j)}|}}I, \tag{10.10}$$

where

$$I=\int\exp(i\pi/4)\sqrt{\frac{\omega\delta\epsilon}{2\pi c_0(\epsilon+\delta)}}\exp\left(\frac{i\omega}{2}\frac{\partial^2\bar{\phi}}{\partial\theta^2}(\theta_j;x_R)\frac{\xi_p\xi^2}{(\xi_p-\xi)}\right)\frac{d\theta}{d\xi}d\xi. \tag{10.11}$$

For the ϵ of (10.4) we can use the approximations of (10.7)–(10.9) in (10.11) to get

$$I\sim\int\left(\frac{-i\omega\delta_j^2}{2\pi c_0(\theta\delta_j'-i\beta\delta_j)}\right)^{1/2}\exp\left(\frac{i\omega}{2c_0}\frac{\delta_j^2\theta^2}{(\theta\delta_j'-i\beta\delta_j)}\right)d\theta. \tag{10.12}$$

Introduce the dimensionless variable σ,

$$\sigma=\frac{\omega}{c_0}\beta\,\delta_j(\delta_j/\delta_j')^2>0 \tag{10.13}$$

then (10.12) becomes

$$I\sim\frac{-i\sigma^{1/2}}{2\pi}\int_{-\infty}^{\infty}\exp\left(i\frac{\sigma}{2}\frac{\bar{\theta}^2}{\bar{\theta}-i}\right)\frac{1}{\sqrt{\bar{\theta}-i}}d\bar{\theta}. \tag{10.14}$$

The integral in (10.14) is zero for $\sigma<0$ and is evaluated in Appendix A for $\sigma>0$ as

$$I\sim1+\exp(-2\sigma) \tag{10.15}$$

We see from (10.10) and (10.15) that the effect of the pole in the phase is to give a field contribution of $[1+\exp(-2\sigma)]$ times that of ordinary ray theory. Note that the factor is a real number between 1 and 2. In the limit $\omega\to\infty$, we have $\sigma\to\infty$ and the factor becomes unity. The factor tends to two as $\epsilon\to-\delta_j$. The factor has been verified from numerical beam integrals with ϵ chosen close to $-\delta_j$. However, as ϵ approaches $-\delta_j$, the numerical integration mesh must be finer and finer in θ. This requires a very dense fan of rays. As an example, consider the cylinder of Section 5 with $D=2000$, $a=500$ and the receiver offset at 2000. For this geometry, we find $\delta/\delta'=3.94$. With $\beta=0.001$ and a frequency of 10 Hz, the factor $1+\exp(-2\sigma)$ is equal to 1.66, whereas the ratio of the beam solution to the ray solution is 1.79. At a frequency of 40 Hz, these two numbers are 1.20 and 1.26, respectively. However, on the order of 10000 rays over a range of 5° were required to ensure numerical stability of the beam solution.

11 Conclusions

We have applied the mathematical theory of uniform asymptotic expansions to explain the behaviour of the Gaussian beam summation method. We have illustrated our theory with numerical calculations of simple generic problems for which exact solutions are obtainable by other means.

We have confirmed the utility of the beam method for computation near caustics, showing how the method constructs correctly the entire caustic boundary layer of a caustic of arbitrary complexity. We have also shown how the method computes correctly near the critical reflection.

For head waves and edge diffraction our results are less encouraging. While the beam integral is of the correct canonical form, the governing parameters are explicitly ϵ-dependent and hence, in general, wrong. For our examples, head waves are given correctly only as $\epsilon\to\infty$, edge diffraction only as $\epsilon\to0$. For more complex problems, e.g. problems involving both of these phenomena, it would be difficult to find a single ϵ that would work.

The presence of strong lateral inhomogeneities further complicates the choice of ϵ. We have shown how, if ϵ is not in an appropriate region of the complex plane, spurious saddle points can arise in the beam superposition integral and degrade the beam solution. Again, multiple arrivals in a single problem would necessitate a compromise between different possible ϵ choices.

We have been unable to propose an algorithm that could handle all these effects, and combinations of them, automatically. Still with an understanding of the problem being solved, the Gaussian beam summation method may be used with advantage.

Acknowledgments

We would like to thank Balan Nair and Kirk Jordan for their help with the numerical computations, and Pravin Shah of Exxon Production Research Company for suggesting this problem to us, and for his continuing encouragement.

References

Abramowitz, M. & Stegun, I. A., 1964. *Handbook of Mathematical Functions*, Applied Mathematics Series 55, National Bureau of Standards.

Bleistein, N. & Handelsman, R. A., 1975. *Asymptotic Expansions of Integrals*, Holt, Rinehart and Winston, New York.

Ben-Menahem, A. & Beydoun, W., 1985. Range of validity of seismic ray and beam methods in general inhomogeneous media, I, *Geophys. J. R. astr. Soc.*, 82, 207–234.

Beydoun, W. & Ben-Menahem, A., 1985. Range of validity of seismic ray and beam methods in general inhomogeneous media, II, *Geophys. J. R. astr. Soc.*, 82, 235–262.

Brekhovskikh, L. M., 1980. *Waves in Layered Media*, Academic Press, New York.

Červený, V., 1983. Synthetic body wave seismograms for laterally varying layered structures by the Gaussian beam method, *Geophys. J. R. astr. Soc.*, 73, 389–426.

Červený, V., 1985. Gaussian beam synthetic seismograms, *Geophysics*, 58, 44–72.

Červený, V., Popov, M. M. & Pšenčík, I., 1982. Computation of wave fields in inhomogeneous media – Gaussian beam approach, *Geophys. J. R. astr. Soc.*, 70, 109–128.

Choudhary, S. & Felsen, L., 1974. Analysis of Gaussian beam propagation and diffraction by inhomogeneous wave tracking, *Proc. IEEE*, 62, 11.

Cormier, V. E. & Spudich, P., 1984. Amplification of ground motion and waveform complexity in fault zones: examples from the San Andreas and Calaveras faults, *Geophys. J. R. astr. Soc.*, 79, 135–152.

Deschamps, G. A., 1971. Gaussian beam as a bundle of complex rays, *Electronics Lett.*, 7(23), 684–685.

Felsen, L. B., 1976. Evanescent waves, *J. opt. Soc. Am.*, 66, 751–760.

Felsen, L. B., 1984. Geometrical theory of diffraction, evanescent waves, complex rays and Gaussian beams, *Geophys. J. R. astr. Soc.*, 79, 77–88.

Gottlieb, D. & Turkel, E., 1976. Dissipative two-four methods for time-dependent problems, *Math. Comput.*, 30, 703–723.

Gradshteyn, I. S. & Ryzhik, I. M., 1980. *Table of Integrals, Series and Products*, Academic Press, New York.

Hubral, P., 1980. Wave front curvatures in 3-D laterally inhomogeneous media with curved interfaces, *Geophysics*, 45, 905–913.

Keller, J. B., 1958. Surface waves on water of non-uniform depth. *J. Fluid Mech.*, 4, 607–614.

Keller, J. B. & Streifer, W., 1971. Complex rays with an application to Gaussian beams, *J. opt. Soc. Am.*, 61, 40–43.

Keller, J. B., Lewis, R. M. & Seckler, B. D., 1957. Diffraction by an aperture, II. *J. appl. Phys.*, 28, 570–579.

Konopaskova, J. & Červený, V., 1984. Numerical modelling of time harmonic seismic wave fields in simple structures by the Gaussian beam method, Parts I and II, *Studia Geoph. Geod.*, 26, 19–35, 113–128.

Ludwig, D., 1966. Uniform asymptotic expansions at a caustic, *Comm. Pure Appl. Math.*, 19, 215–250.

Madariaga, R., 1984. Gaussian beam synthetic seismograms in a vertically varying medium, *Geophys. J. R. astr. Soc.*, 79, 589–612.

Morse, P. M. & Feshbach, H., 1953. *Methods of Theoretical Physics*, McGraw-Hill, New York.

Müller, G., 1984. Efficient calculation of Gaussian beam seismograms for two-dimensional inhomogeneous media, *Geophys. J. R. astr. Soc.*, 79, 153–166.

Nowack, R. & Aki, K., 1985. The 2-D Gaussian beam synthetic method: testing and application, *J. geophys. Res.*, 89, 7797–7819.

Popov, M. M., 1982. A new method of computation of wave fields using Gaussian beams, *Wave Motion*, 4, 85–92.

Sommerfeld, A., 1954. *Optics, Lectures on Theoretical Physics*, Vol. IV, Academic Press, New York.

Sommerfeld, A., 1896. *Math. Ann.*, 47, 317.

Appendix A: Evaluation of (10.14) for $\sigma > 0$

First change the integration variable to $\xi = \bar{\theta} - i$ and choose the branch cut of $\sqrt{\xi}$ to be the positive imaginary axis. Then

$$I \sim \sqrt{\frac{-i\sigma}{2\pi}} \exp(-\sigma) \int_C \exp\left[i\frac{\sigma}{2}\left(\xi - \frac{i}{\xi}\right)\right] \frac{d\xi}{\sqrt{\xi}}. \tag{A1}$$

The integration path is any contour that goes from $\xi = i\infty - 0$ to $\xi = i\infty + 0$ around the branch cut. Split C into two separate contours C_1 and C_2 with corresponding integrals $I^{(1)}$ and $I^{(2)}$. Let C_1 be the union of the straight line contours from $i\infty + 0$ to $i - 0$ and from $i + 0$ to $i\infty + 0$. Then

$$I^{(1)} = \sqrt{\frac{\sigma}{2\pi}} \exp(-\sigma) \int_i^{i\infty} \frac{-2i}{\sqrt{|\xi|}} \exp\left[i\frac{\sigma}{2}\left(\xi - \frac{1}{\xi}\right)\right] d\xi$$

$$= \sqrt{\frac{\sigma}{2\pi}} \exp(-\sigma)\, 2 \int_0^\infty \exp\left(-\sigma\cosh t + \frac{t}{2}\right) dt \tag{A2}$$

and from Abramowitz & Stegun (1964, equation 9.6.20) we have

$$\int_0^\infty \exp\left(-\sigma\cosh t + \frac{t}{2}\right) dt = \pi I_{-1/2}(\sigma) - \int_0^\pi \exp(\sigma\cos\theta)\cos\frac{\theta}{2} d\theta, \tag{A3}$$

where $I_{-1/2}$ is the modified Bessel function of the first kind of order $(-1/2)$. It follows from Abramowitz & Stegun (1964) that

$$I_{-1/2}(\sigma) = \sqrt{\frac{2}{\pi\sigma}} \cosh\sigma. \tag{A4}$$

The second contour C_2 goes from $i - 0$ to $i + 0$ in a counter-clockwise sense on the unit circle. Thus,

$$I^{(2)} = \sqrt{\frac{\sigma}{2\pi}} \exp(-\sigma) \exp\left(\frac{i\pi}{4}\right) \int_{-3\pi/2}^{\pi/2} \exp\left(\frac{i\phi}{2}\right) \exp(-\sigma\sin\phi)\, d\phi$$

$$= \sqrt{\frac{\sigma}{2\pi}} \exp(-\sigma)\, 2 \int_0^\pi \exp(\sigma\cos\theta)\cos\frac{\theta}{2} d\theta. \tag{A5}$$

We then have

$$I \sim I^{(1)} + I^{(2)} \tag{A6}$$

which, along with (A2)–(A5), implies (10.15).

Appendix B. Finite difference computation for the syncline of Section 5

For the parameters considered in Section 5, it was necessary to follow the solution for a distance of the order of 20 wavelengths, based on the peak frequency of the source pulse. In addition, the frequency spectrum was shifted into higher frequencies since the source pulse was essentially a second derivative of a Gaussian (thus the propagating pressure had a frequency spectrum characteristic of a 3/2th derivative of a Gaussian). It was our experience that standard second order finite difference schemes were not satisfactory in obtaining solutions of the required accuracy.

The solutions were computed by finite difference schemes which were second order accurate in time and fourth order accurate in space [(2–4) schemes]. A heterogeneous formulation was used whereby the solution was differenced across the interface. In 2-D there are not theoretical results regarding the accuracy of this technique (in particular there is no theory relating the effects of curvature to the accuracy of the discretization). The careful benchmarking of the finite difference computation with the other solution techniques therefore had the additional benefit of establishing the accuracy of the discretization schemes in the presence of curvature.

The numerical solution was computed with two different (2–4) schemes. The first scheme was based on the second order wave equation for the acoustic pressure

$$P_{tt} = \rho c^2 \left[\left(\frac{P_x}{\rho}\right)_x + \left(\frac{P_y}{\rho}\right)_y \right] \tag{B1}$$

The standard fourth order approximation for the function $[(1/\rho)P_x]$ is

$$\left(\frac{1}{\rho}P_x\right) \approx \frac{4}{3h^2}\left(\frac{1}{\rho_{i+1/2}}(P_{i+1} - P_i) - \frac{1}{\rho_{i-1/2}}(P_i - P_{i-1})\right)$$

$$-\frac{1}{12h^2}\left(\frac{1}{\rho_{i+1}}(P_{i+2} - P_i) - \frac{1}{\rho_{i-1}}(P_i - P_{i-2}).\right) \tag{B2}$$

In (B2) h is the mesh size and the subscript i is an index for the x grid. A similar formula holds for the term $[(1/\rho)P_y]$. These spatial approximations can be combined with the standard second order approximation to P_{tt}

$$P_{tt} \approx \frac{P^{n+1} + P^{n-1} - 2P^n}{\Delta t^2},$$

where Δt is the time step, to obtain the (2–4) approximation to (B1).

The second scheme is based on the linearized first order system for acoustic fluctuations

$$\rho U_t = -P_x$$

$$\rho V_t = -P_y$$

$$P_t = -\rho c^2(U_x + V_y), \tag{B3}$$

where U and V are the horizontal and vertical velocities respectively and P is the pressure. An effective (2–4) scheme for (B3) is obtained by operator splitting. The solution is updated schematically as follows:

$$w^{n+2} = L_x L_y L_y L_x w^n$$

Here w^n is the vector $(U, V, P)^T$ at time level n and L_x and L_y are approximations to the 1-D equations

$$\rho U_t = -P_x,$$

$$P_t = -\rho c^2 U_x; \tag{B4}$$

and

$$\rho V_t = -P_y$$

$$P_t = -\rho c^2 V_y.$$

An approximate (2–4) scheme for a 1-D equation of the form (B4), written symbolically as $w_t = f_x$, is

$$\bar{w} = w^n + \frac{\Delta t}{6\Delta x}\,[7(f_{i+1} - f_i) - (f_{i+2} - f_{i+1})]$$

$$w^{n+1} = \frac{1}{2}(w^n + \bar{w} + \frac{\Delta t}{6\Delta x}\,[7(\bar{f}_i - \bar{f}_{i-1}) - (\bar{f}_{i-1} - \bar{f}_{i-2})]$$

together with a symmetric variant (see Gottlieb & Turkel 1976).

Careful numerical experiments for both the syncline and the circular cylinder discussed in Section 6 have demonstrated that both schemes give very similar results and are significant improvements over second order discretizations. In particular, the numerical results presented in Section 5 can be regarded as sufficiently accurate to assess the effectiveness of the asymptotic methods.